ISTITUTO NAZIONALE DI FISICA NUCLEARE

Report: Fundamental Physics at Frascati(*)

Fabio Bossi, Paola Gianotti, Enrico Nardi

Editors

INFN, Laboratori Nazionali di Frascati, C.P. 13, I-00044 Frascati, Italy

Abstract

This report summarizes the scientific discussion of the workshop "Fisica Fondamentale a Frascati" that was held on January the 13th, 2021.

The aim of the meeting was to brainstorm on the opportunities to continue to carry out at the LNF experimental activities that could contribute to the scientific exploration of fundamental open questions in particle physics. This initiative has been triggered by the awareness that while the ongoing DAΦNE scientific program is coming to an end, the EuPRAXIA project, identified as the major future activity of the LNF, has a time horizon of several years before entering the operation phase. Therefore, we asked ourselves to which fields in fundamental physics the LNF can give a sound contribution within the medium-term by exploiting the existing infrastructures or, in case some breakthrough for some specific research is foreseeable, by implementing minor upgrades. The topics that have been identified are: (i) the quest for dark matter candidates in terms of feebly interacting light particles; (ii) probing the axion solution to the strong CP puzzle by searching for dark matter axions with superconducting cavities and with large volume haloscopes; (iii) the study of the low energy QCD problems related to the role of strangeness in nuclear matter. Theoreticians and experimentalists convened to scrutinize the different aspects of these scientific issues.

The format chosen for the workshop foresaw a theory talk introducing each subject, followed by experimental contributions describing in detail how the scientific goal can be best addressed.

This document resumes the various contributions in a condensed form, and is intended to provide a guideline for who will be asked to evaluate this program. Additional material can be found at the webpage of the meeting (https://agenda.infn.it/event/25299/).

(*) This document is a collaborative effort which includes, but is not restricted to, Danilo Babusci, Fabio Bossi, Catalina Curceanu, Luc Darm, Claudio Gatti, Paola Gianotti, Carlo Guaraldo, Venelin Kozhuharov, Carlo Ligi, Enrico Nardi, Isabella Oceano, Kristian Piscicchia, Mauro Raggi, Diana Sirghi, Alessandro Scordo, Paolo Valente, Johann Zmeskal.
Email addresses: fabio.bossi@lnf.infn.it (Fabio Bossi), paola.gianotti@lnf.infn.it (Paola Gianotti), enrico.nardi@lnf.infn.it (Enrico Nardi)

Contents

1. Fundamental Physics at Frascati (*Fabio Bossi*)

The Frascati National Laboratory of INFN, LNF, has always been at the forefront of scientific research in the field of high energy particle accelerators development and in that of fundamental particle physics experiments. These two fields have strongly overlapped, already since the times of the first e^+e^- collisions at ADA, as well as in more recent times with the still ongoing experimental activity at the DAΦNE collider.

With the recent approval of the EuPRAXIA project the LNF is entering a new era. Whithin less than a decade a new machine will be built, with the ambitious goal of being the first user facility that exploits plasma acceleration. This machine will serve a vast community of users, which however will hardly be interested in fundamental physics issues. In the forthcoming years most of the financial, technical and manpower resources of the laboratory will necessarily be dedicated to this project.

Having this clear in mind, there is, however, a key question that needs to be addressed:

Is there a sound experimental physics program that can be performed using the existing scientific infrastructures of the laboratory and can produce top-class results in some well-identified fundamental physics field in the short-medium term, i.e. before the start of operations of EuPRAXIA?

This question is strictly related to another very important one:

What future usage, if any, can be envisaged for the DAΦNE accelerator complex after the end of the SIDDHARTA-2 run?

Given the time framework presented above, it is clear that an answer to these questions must be given quickly, i.e. on a time scale of the order of about one year. A decision-making process in this direction has been elaborated, divided in three well identified steps.

1. Determination of the physics projects that can provide a positive answer to the first question above, together with the identification of the community that intends to pursue them.
2. Determination of the impact of these projects on the laboratory, in terms of financial and manpower resources; this implies also the evaluation of the interference of the proposed projects with the development of EuPRAXIA and of the many activities related to it.
3. Discussion with the INFN Management about the potential interest in endorsing one or many of these projects to arrive to a final operational decision.

The workshop *"Fisica Fondamentale a Frascati"* (FFF) was primarily intended to address the first step above. Three experimental programs were discussed in some detail. All of them are rather mature and have been discussed in the past in other occasions. We have decided to collect the relevant information of these presentations in this report, with the purpose of allowing the readers, most notably the LNF Scientific Committee members, to set up their minds about the scientific pros and cons of each of them.

In all three cases, firstly a brief introduction to the physics motivations is given, followed by a discussion on the experimental activity that could be potentially performed. All the three activities can be declined into different options, of different scales of complexity. All of them have a time-horizon which reasonably fits our requirement. Two of them are supposed to be carried out at DAΦNE ; their mutual interference is therefore obvious.

At the stage of step 1, we expect to obtain an evaluation about the physics interest of these proposals and of their impact in the related fields. We ask the Scientific Committee of LNF to provide an independent, authoritative opinion on this. The evaluation of step 2 will proceed in parallel, and will be a matter of discussion on another occasion, yet to be decided.

2. Feebly interacting light particles

2.1. Feebly interacting light particles: motivations and hints (Enrico Nardi)

One of the most compelling arguments motivating the search for extensions of the Standard Model (SM) is the need to explain the nature of dark matter (DM). In years past, theoretical and experimental efforts mainly catalysed around the hypothesis that DM corresponds to a Weakly Interacting Massive Particle (WIMP) with electroweak scale mass. Such a hypothesis is well grounded since in the early Universe WIMPs would be produced via thermal processes, and their annihilation with typical weak interaction rates would leave, almost independently of other details, a relic density of the correct size to explain DM observations. However, despite an extensive search program that combined direct, indirect, and collider probes, to date no conclusive signal of the WIMP has been found [1]. This prompts the scientific community to put no lesser vigor in exploring alternative pathways.

Feebly interacting particles (FIPs) represent a particularly interesting alternative to WIMPs. In recent years the physics of FIPs has focused a steadily growing interest, as it is witnessed by the remarkable number of community reports and white papers that appeared in the last few years [2–7]. FIPs are exotic and relatively light particles, not charged under the SM gauge group, whose interactions with the SM bosons or fermions are extremely suppressed. FIPs are often assumed to be part of a possibly complicated secluded sector, called the *dark sector*, with the lightest stable dark particle(s) playing the role of DM. This scenario has sound theoretical motivations: in first place many known particles are uncharged under some gauge group factors, so that the existence of particles blind to all $SU(3)_C \times SU(2)_L \times U(1)_Y$ interactions seems a rather natural possibility. Secondly, theoretical mechanisms like gauge symmetries or quasi-exact spontaneously broken global symmetries, that we know are realised in Nature, can explain why some particles remain light even when they are associated with physics at some large scale: a zero-mass photon is generated upon spontaneous breaking of the electroweak symmetry associated with $\Lambda_{\mathrm{EW}} \sim 100\,\mathrm{GeV}$, pions are the Goldstone-bosons of a global symmetry broken spontaneously at a scale $\Lambda_{\mathrm{QCD}} \gg m_\pi$. From the phenomenological point of view, light weakly coupled new particles have been often invoked to account for several discrepancies observed in low energy experiments. Examples are the measured value of the muon anomalous magnetic moment [8], the proton charge radius measured in muonic atoms [9–11], the discrepancy between neutron lifetime measurements in bottle and beam experiments [12, 13], the measured abundance of primordial ^{7}Li which is a factor of three lower than BBN predictions [14], the 'bump' in the angular distribution of $e^\pm$ pairs observed by the Atomki collaboration in nuclear decays of ^{8}Be [15] and ^{4}He [16] excited states.

FIPs scenarios hint to a remarkably broad range of possibilities, ranging from the very nature of the new particles (scalars, pseudoscalars, fermions, spin-one bosons) and spanning several order of magnitude in mass and couplings. To thoroughly explore all these possibilities will require an extensive collaboration among a variety of small/medium scale experiments, exploiting diversified detection techniques, and operating at different facilities. This was emphasised in the 2020 Update of the European Strategy for Particle Physics [17] that states: *"the role of the National Laboratories in advancing the exploration of the lower energy regime cannot be over-emphasised"* and where a specific mention to FIPs searches at LNF was also included *"...a search for low-mass dark matter particles with a positron beam is under way at Frascati...These initiatives should be strongly encouraged and supported"*. The LNF accelerator facilities are in fact utterly adequate to contribute to this venture. To give an example, among all existing facilities the DAΦNE complex is probably the best suited to confute or validate the particle physics explanation of the Atomki anomaly [15, 16], which requires a dark boson (dark photon or axion-like particle, aka ALP) with a mass around 17 MeV. The Frascati BTF can deliver positrons that can annihilate with target atomic electrons with a c.o.m. energy spanning the interval $15 - 23\,\mathrm{MeV}$. This covers the range in which the dark boson can be produced resonantly, yielding a huge enhancement in the production rate. In fact, it is precisely because of the availability of a positron beam that the process of resonant FIPs production was first identified and studied in Frascati [18]. It is now recognised that this process is of general importance since, due to the presence of secondary positrons in EM showers, it contributes to FIPs production also in electron [19, 20] and proton [21] beam experiments, and hence it must always be included when studying light DM production at colliders. However, it is especially for positron beam fixed target experiments that, assuming a proper experimental setup, the role of resonant annihilation for FIPs searches would become decisive [22].

2.2. Options for improvements of the LNF e^+/e^- beam (Paolo Valente)

The common rationale of all options here briefly described is to increase the reach of experiments searching for light feebly interacting particles (FIP) by improving the existing LNF accelerator facilities. Only modifications to the DAΦNE complex are discussed, due to the lower maximum energy and the lack of positron production of the SPARC-lab LINAC. Two additional criteria have been considered: first of all, the proposed solutions should allow keeping in operation the Beam-Test Facility lines and of the DAFNE-Light synchrotron laboratory; secondly, in order to be completed in the short-medium term, they should be projects of the scale of the BTF doubling [23, 24] in terms of complexity, cost and required personnel.

The requirements of two different types of experiments have been considered: **electrons on thick dump** (see for instance [19]), needing the highest possible energy and intensity electron beam, regardless of its time structure; and **positrons on thin target** [25], demanding the highest possible energy and diluted in time positron beam, with small (well below 1%) momentum spread and good emittance. The reference parameters for the present performance of the DAΦNE LINAC are respectively: the high-intensity irradiation tests occasionally performed at BTF with primary electrons [26], up to an intensity of $1.5 \cdot 10^{10}/10$ ns pulse [27], and the operation with long pulses of primary positrons in 2019-2020 PADME experiment run [28].

For the first class of electron beam dump experiments, there are two basic limitations: one comes from the radioprotection issues which are strongly depending on the location of the setup, the other is the maximum available beam charge from the LINAC. Assuming to dump the primary LINAC beam in the BTF-1 hall, where the PADME experiment is currently installed, the maximum allowed average intensity over a yearly basis is $3.125 \cdot 10^{10}$ particle/s at the maximum energy of 800 MeV [29], corresponding to $9 \cdot 10^{17}$ particles/year. This intensity can be easily exceeded already with relatively short LINAC pulses. The limit is even lower (four orders of magnitude with the present shielding) for the new BTF-2 bunker. In order to exploit the maximum charge that the LINAC can deliver, there are two alternatives: extracting the beam onto the existing beam-dump the end of the LINAC (keeping off the DHPTT01 dipole), or using the shielded hall of the accumulator ring, once it will be no longer used for DAΦNE injections. Extending the pulse length a constant current can be extracted from the thermoionic gun, so that a beam charge linearly increasing with a slope ≈ 0.2 nC/ns can be accelerated by the RF structures [30]. No saturation has been observed up to the maximum sensitivity of the LINAC diagnostics (10 nC), so that at the maximum already achieved length of 350 ns [31] up to 70 nC could be obtained. Even with a lower maximum accelerating field achievable with such long pulses, a maximum energy for primary electrons of **670 MeV** has been achieved. In terms of electrons on target (eot) with the convention (also assumed in the following) of an equivalent year of 10^7 s, this corresponds to a potential statistics for an electron dump experiment of the order of $\mathbf{2 \cdot 10^{20}}$ **eot/year**, at the maximum repetition rate of 49 s^{-1}.

For positron on fixed-target experiments, two techniques have been considered: missing mass searches in $e^+ e^- \to \gamma X$ (being X a generic FIP) and missing momentum/energy experiments (as described in Sec. 2.5). In both cases the main parameter to be improved is the length of beam pulse, in order to allow a higher beam intensity without increasing the particle density, assuming that the detector technology will be the same as (or similar to, in case of a completely new setup) the PADME experiment. While in the first case the maximum tolerable pile-up and veto probability limit is set to a reference figure of 10^2 positrons/ns [32], in the latter the objective is to track beam particles one-by-one, which essentially fix the maximum density to one positron every ~ 10 ns, taking as a reference a double-pulse separation of ≈ 2 ns [33] of the PbF$_2$ Cherenkov detector of PADME. The maximum achievable statistics under these basic assumptions **on the experiment performance**, expressed in positrons on target (pot) is: $10^{18} \times d$ pot/year for the thin-target option, and $10^{15} \times d$ pot/year for a missing momentum experiment, being d the effective duty-cycle. As a reference, the maximum beam length during the PADME runs reached ≈ 320 ns at the maximum 49 s^{-1} rate, corresponding to an effective duty-cycle of $d = 1.5 \cdot 10^{-5}$, i.e. potentially to $\mathbf{1.5 \cdot 10^{13}}$ **pot/year**. The maximum achieved positron beam energy with such long pulses was **490 MeV**. In the following possibilities for getting significantly longer positron pulses with the required intensity, at the expense of the maximum energy are briefly described: a minimum beam energy of ≈ 282 MeV is however desirable, in order to still allow the production of the hypothetical X17 boson in $e^+ e^-$ fixed target annihilations.

5

2.2.1. Extending the positron beam produced by the LINAC

Electrons and positrons are accelerated by 3 m long, SLAC-type, S-band travelling wave, constant gradient sections – five before and 10 after the positron production target – fed by four RF stations. The 4.5 μs long flat pulse produced by the 45 MWp klystrons is compressed by means of a device (SLED), which store the RF power in two cylindrical TE_{015} cavities coupled by a 3 dB hybrid, and then releases it to the sections with a peaked shape, thus allowing to reach a higher accelerating field (gain factor $\approx$ 1.6) [34]. In order to produce beam pulses much longer than 10 ns, required for injection into the DAΦNE rings, the power and phases of the four modulators have to be adjusted for smoothing the RF peak, at the price of a slightly lower maximum energy and larger spread as described in Ref. [31]. In order to accelerate pulses much longer than 350 ns, while keeping the momentum spread at a few % level in order to match the BTF beam-line acceptance, the idea is to remove the SLED compression.

Among the several methods proposed in Ref. [35], the two basic options are: to totally by-pass the cavities or to flatten the output power by modulating the low-level RF (LLRF) source. In the first case, the by-pass can be performed either physically, i.e. connecting directly the klystron output to the waveguide network distributing the power to the LINAC sections, or by preventing the power to be stored into the SLED cavities. This can be done by bringing them far from the resonance frequency, e.g. through the complete insertion of the thin Tungsten rod generally used for the fine-tuning. In both cases, the natural, flat RF pulse from the klystron would be directly fed to the accelerating sections. Taking into account the filling time of the accelerating structures of $\approx$ 830 ns [34], it should be possible to accelerate up to **3 μs** long positron pulses, corresponding to an increase of one order of magnitude on the duty-cycle, $d = 1.5 \cdot 10^{-4}$. Due to the absence of the SLED compression, the maximum energy would be $\sim$**300 MeV**. The second option does not modify the basic hardware configuration of the RF stations: a flat power after the phase inversion driving the RF discharge to the sections can be obtained by modulating the LLRF phase and/or amplitude, by means of a dedicated FPGA-based module [36]. Assuming a reduction of 50% of the energy gain with respect to full compression, **800 ns** long ($d = 4 \cdot 10^{-5}$), $\sim$**420 MeV** positron pulses can be produced. In both options, the fairly flat accelerating field should also produce an energy spread well below 1%.

2.2.2. Using a ring as pulse stretcher of the LINAC

Another possibility for extending the bunch length from a pulsed LINAC is to use a synchrotron ring as stretcher. The POSEYDON proposal [37] is to use one of the two main rings of the DAΦNE collider, in particular the positron one, thus allowing to keep in operation the synchrotron beam-lines installed on the electron ring. The basic idea is the same of several past electron LINAC pulse-stretcher proposals, starting from ALIS [38] at Saclay ALS 300, followed by ALFA [39] at LNF ADONE, later implemented in the EROS ring [40] at Saskatchewan. The scheme is the following: long LINAC pulse are injected into the ring, in order to be slowly extracted by the so-called resonant extraction. This is a well know technique, mainly implemented in hadron machines, consisting in setting the betatron tune close to an integer resonance, creating a limited region of stability in the horizontal (x, x') phase space. In the case of the most commonly used third of integer resonance, the stable region has a a triangular shape. Particles close to one of the sides of the triangle – the so-called "separatrix" – are unstable, and turn after turn will be driven outwards, until they intercept an extraction septum. In order to keep extracting, more particles should be driven to the unstable region: the standard method for hadrons is to shrink the stable triangle, moving the tune closer and closer to the resonance, typically by means of a quadrupolar variable field. For circulating electrons (or positrons) it is possible to go towards the resonance profiting of the continuous energy loss due to synchrotron emission. Provided that the chromaticity ξ of the ring is not zero and the RF is kept off, this translates the energy change in a tune change: $\Delta\nu/\nu = \xi\Delta p/p$. The extraction will be thus completely determined by the energy spread of the beam, and will take place at a defined energy value, so that it is also called "monochromatic". In the case of the DAΦNE, assuming to inject at $\Delta p/p = +0.5\%$ and extracting at -0.6%, if the energy loss is reduced energy to 4.5 keV/turn by keeping the wigglers off, a septum placed at 40 mm from the reference orbit would be reached in 1400 turns [41], so that **0.45 ms** pulses can be obtained at $E = $ **510 MeV**, corresponding to a duty-cycle $d = 0.02$. Even considering the need of some collimation for controlling the emittance and spread of the injected beam, the required intensity of extracted positrons should be easily obtained starting from $> 10^{10}$, 300 ns pulses (being 324 ns the revolution time of the ring).

The nominal energy is very close to the maximum achievable positron energy with such long beam from the LINAC, and also the ring dipoles are already close to the maximum field due to iron saturation. Since the mass reach of fixed-target positron annihilations searches of dark particles only scales with $\sqrt{E}$, it would be still interesting to perform the extraction at a lower E: while the total loss ΔE decreases linearly (for a fixed relative spread), the synchrotron loss scales as E^4, so that the net result will be a significantly longer extraction time. For instance a spill of **0.9 ms** at **400 MeV** and **2 ms** at **300 MeV** is expected.

This solution requires several modifications to the DAΦNE complex. First of all an electrostatic septum providing a first small angle kick is needed, followed by a magnetic one bending the beam towards an extraction line. In order to profit for the larger possible horizontal offset at the septum the optimal location along the ring would be in a position where the β function reaches its maximum, since the oscillation amplitude is $\propto \sqrt{\beta}$, thus minimizing the losses: e.g. for a step of 5 mm, losses at the level of 2% are expected for a 0.1 mm thick septum [41]. In the standard optics for DAΦNE (shown in Fig. 1), this is verified in the long straight sections connecting the ring arcs, where the dispersion is also vanishing, thus minimizing the extracted beam emittance. The extraction line should bring the positron beam far enough from the ring to accomodate the experimental setup, while preserving the momentum spread, which is expected to be small thanks to the monochromatic extraction, and can be as simple as an achromatic dogleg. Due to the less stringent requirements on the injected bunches, the long LINAC pulses can be injected directly, without passing through the intermediate, small ring (also called "accumulator"). A small angle pulsed dipole plus a larger DC bending would be sufficient to divert the beam from the LINAC transfer-line to the main rings hall. Such a scheme would also allow efficient injection of bunches in the electron ring, thanks to an emittance as good as $\varepsilon_{x,y}^{rms} \approx 10^{-7}$ [42], for the independent operation of DAFNE-Light. Finally, injecting ≈ 300 ns macro-bunches in the positron ring will also requires longer kicker pulses.

An alternative approach to an electrostatic thin septum (typically wires) is to use coherent processes in a bent crystal for displacing the positrons. There a number of phenomena occurring when a charged particle hits a regular lattice with a given curvature, which have been extensively studied for beam manipulation [43]. Those studies have been mainly performed with high energy hadrons, but a number of results have been also obtained with electrons and positrons, also in the sub-GeV energy range: in particular channeling [44, 45], volume reflection [46] and mirroring [47] can provide a significant beam deflection with a good efficiency. The SHERPA project [48], funded by grant of INFN CSN-5, is aimed at investigating the possibility of using a bent crystal for complementing and improving the resonant extraction. The advantage of dealing with positively charged particles is the possibility of using the simpler "planar" channeling, profiting of particle oscillations between the atomic lattice planes, with respect to "axial" coherent effects due to the interaction with an atomic string along a crystallographic axis. The latter are more relevant for the deflection of negative particles [49], for which the planar channeling is much less efficient, and have more stringent alignment conditions. The peculiarity of such a technique is the possibility of implementing a non-local extraction: i.e. the beam is not directly driven out of the ring pipe though the first septum, but instead the crystal imparts an angular kick to the particles crossing it, making them follow different oscillations until they are displaced enough to reach a further deflection, given for instance by a magnetic septum, after a given phase advance or even some turns. A critical difference with respect to the high-energy hadron case, is the not negligible contribution of the Coulomb multiple scattering of un-channeled particles, which calls for a thin crystal. However, dealing with lower momentum (p) particles implies a larger critical angle, $\theta_c \propto \frac{1}{\sqrt{p}}$, and thus a larger acceptance (at 510 MeV in a Si(110) crystal $\theta_c \approx 290$ μrad [50]). For maximum channeling efficiency the curvature radius of the crystal has to be much larger than a critical value R_c, which scales linearly with p: at 510 MeV for for Si(110) $R_c \sim 0.9$ mm. This limits the bending angle, for a given thickness L, to less than $L/(n \cdot R_c)$, where a safe value is $n \approx 10$ for Silicon [51]. SHERPA objective is thus to realize a Silicon crystal $L = 30$ μm thick and $\alpha \approx 1$ mrad bending. Preliminary studies [52], indicate that already with a ring optics close to the standard one for collisions [53] (Fig. 1, left), placing the crystal at 8 mm from the reference orbit in a high-β, low dispersion, straight section close one of the two crossings of the main rings, it is possible to get a 20 mm offset (as shown in Fig. 2) after a $\Delta\mu \simeq 0.25$ phase advance, in order to cross an extraction magnetic septum (see the two possible locations in the layout [54] in Fig. 1, right).

In the basic scheme the extraction time is completely determined by the energy loss, so that it would
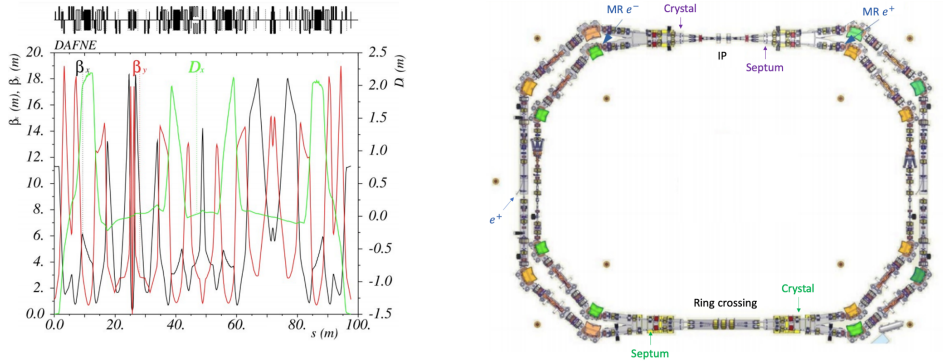
Figure 1: Left: example of optical functions of the DAΦNE main rings for collisions. Right: layout of the DAΦNE main rings with two locations for the crystal and magnetic septum.
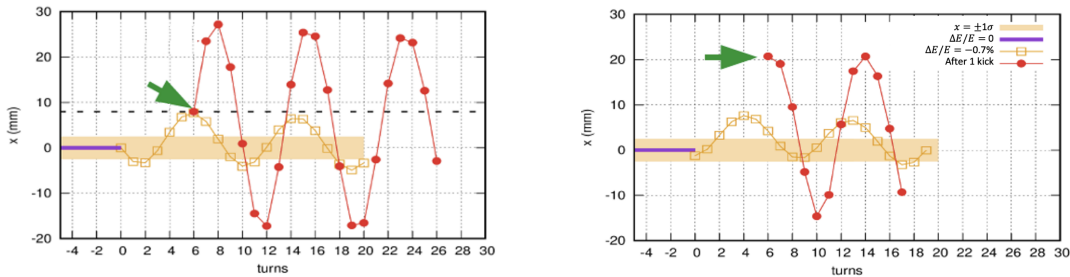

Figure 2: Tracking of positrons at the crystal (left) and at the extraction septum (right) before (yellow square) and after the kick (red dots).

be interesting to modify it in for having some control of, and in case further extending, the spill time. For example, if the radiofrequency of the ring could is kept on, thus leaving the beam inside the bucket, the amplitude of betatron oscillations can be increased by modulating the amplitude or the phase [55].

Even though the monochromatic extraction requires the wigglers and the RF of the positron ring to be off, thus reducing the required power by $\approx 50\%$ (also considering the operation of the electron ring with just one wiggler, for synchrotron light production), it is worth investigating the possibility of using the DAΦNE accumulator [56], which is a much simpler and smaller ring (1/3 of the main ring), as pulse stretcher of the LINAC positron beam. This intermediate ring is generally used for damping LINAC bunches, 10 ns long (RF is 1/5 of the DAΦNE one), prior to be injected into the proper bucket of the main rings. Another advantage with respect to one of the main rings is the presence of two couples of magnetic septa (a straight, thin 2° one [57, 58] and a curved 34° one), alternatively used for injecting and extracting positrons and electrons in the same ring (obviously in opposite directions). The design of the accumulator was aimed at a very large momentum acceptance, its standard optics has relatively small β functions and dispersion, and very small chromaticity. This has to be modified in order to implement the resonant extraction: the first studies [52] show that β_x can be largely increased at the expense of a smaller momentum acceptance of $(-0.5\%, +0.1\%)$. With a proper chromaticity it is possible to find a configuration which produces an offset sufficient to cross the 1.5 mm thick first septum, placed at 20 mm (inwards) from the central orbit, with a $\Delta p/p$ of order 0.6%, after 600 turns, given a synchrotron loss of 5.2 keV/turn. This translates to $\approx \mathbf{60\mu s}$ due to the smaller revolution time. Since this configuration has not been optimized, it is possible to gain at least a factor 2, for instance working closer to the tune resonance or increasing the aperture for injecting out of energy. Also in this case, running at a lower energy will produce longer spills: a factor ≈ 2 going from 510 to 400 MeV, and ≈ 5 working at 300 MeV. Due to the limited space in the accumulator ring building, it will be necessary to drive the beam to a different location, where the experiment can be installed. This can be done by using the same line bringing the LINAC pulses in the opposite direction, following the

Accelerator	Notes	Pulse length	Energy		Particles on target/year	
			Positrons	**Electrons**	**Positrons**	**Electrons**
LINAC	–	300 ns	490 MeV		$1.5 \cdot 10^{13}$	
				670 MeV		$2 \cdot 10^{20}$
LINAC	LLRF modulation	800 ns	420 MeV		$4 \cdot 10^{13}$	
				580 MeV		$5 \cdot 10^{20}$
	De-tuned SLED	3 μs	300 MeV		$1.5 \cdot 10^{14}$	
				460 MeV		$2 \cdot 10^{21}$

Table 1: Summary of parameters for producing positron and electron beams with the DAΦNE LINAC.

path of the standard injection in the main rings. Once having reached the DAΦNE hall, the beam can be then diverted by an additional dipole on the positron injection line (downstream of the dipole DHRTP01). Alternatively, a dedicated, relatively short and simple transfer-line can be realized: if the lateral dimensions of the experimental setup are similar to the PADME ones (≈ 2 m), the nearby hallway connecting the end of the LINAC transfer-line (at the 45° bending DHPTT01) to the accumulator can be used.

Summary of proposed improvements

In Tab. 1 the expected performance of the two main possibility of further extending the electron and positron pulses of the LINAC is reported: the maximum gain in statistics that can be expected with the present machine is of one order of magnitude, at the price of a reduction of the maximum beam energy, for all cases in which the particle density is not an issue, e.g. for a thick target dump experiment. If the present BTF-1 hall is used, the yield will be limited to $9 \cdot 10^{17}$/year (10^7 s) due to the radioprotection authorization. A much larger gain in statistics for a thin target experiment with positrons is instead expected if one of the rings is used as a pulse stretcher. Resonant extraction from the positron main ring seems to yield the best parameters, which can be improved by using crystal channeling, but the alternative of using the smaller and much simpler accumulator ring is also attractive. The two options are compared in Tab. 2. Number of particles on target/year (10^7 s) is referred to a density of 10^2 positrons/ns.

Accelerator	Notes	Pulse length	Duty-cycle	Energy	pot/year
LINAC + main ring	electrostatic septum/crystal + magnetic septum	0.45 ms	0.022	510 MeV	$2 \cdot 10^{16}$
		0.9 ms	0.044	400 MeV	$4 \cdot 10^{16}$
		2 ms	0.1	300 MeV	$1 \cdot 10^{17}$
LINAC + accumulator	crystal + magnetic septa	60 μs	$3 \cdot 10^{-3}$	510 MeV	$3 \cdot 10^{15}$
		120 μs	$6 \cdot 10^{-3}$	400 MeV	$6 \cdot 10^{15}$
		0.3 ms	0.015	300 MeV	$1.5 \cdot 10^{16}$

Table 2: Summary of parameters for producing positron beams using a DAΦNE ring as LINAC pulse stretcher.

2.3. PADME and beyond: prospects at LNF (Venelin Kozhuharov, Mauro Raggi)

2.3.1. PADME physics strategy

The PADME experiment at LNF-INFN [59] employs a positron beam impinging on a very thin target. Only a small fraction of the positrons interact with large momentum transfer with the atomic nuclei or electrons in the target. The rest of the beam respects its initial direction and energy to a large extent and is transported outside the apparatus. The nominal positron beam energy is given by the accelerator and beam transportation setup.

The possible detectable high energy particles in the final state are limited by the beam energy and for $E_{e^+} \simeq 500$ MeV they are just γ, e^+ and e^-. Photonuclear interactions may lead to neutron production but in the case of thin target the neutron flux is negligible.

PADME experiment aims to detect both the high energy photons and the charged particles in the final state. This assured by an electromagnetic calorimetric system and a set of segmented charged particle detectors inside the magnetic field of a dipole. The position information and the magnetic field strength

allow to infer the charged particle momentum, assuming that the emission direction coincides with the beam direction.

Several observational quantities could be reconstructed with the PADME setup:

- *Missing mass:* In the case of the detection of a single final state photon, the missing mass can be determined as

$$M^2_{miss} = (\bar{P}_{e^+} + \bar{P}_{e^-} - \bar{P}_\gamma)^2, \tag{1}$$

  where $\bar{P}_{e^+}$ and $\bar{P}_{e^-} = (m_e, \vec{0})$ are the beam positron and the target electron 4-momenta. The gamma 4-momentum is determined from the interaction point in the target, the energy of the gamma, and its impact position in the electromagnetic calorimeter.

- *Invariant mass:* In the presence of more that one final state photon the invariant mass can be reconstructed, assuming they originate from the impact point of the beam in the target:

$$M^2_{inv} = (\bar{P}_{\gamma_1} + \bar{P}_{\gamma_2} + \dots)^2 \tag{2}$$

  The invariant mass quantity is independent on the beam parameters and provides an extra constraint in different physics channels, allowing for precise background determination and control.

- *Charge particle multiplicity:* The charged particle detectors do not allow for precise momentum reconstruction, however their segmentation provides multiplicity information momentum estimation with better than 10 % accuracy. The charged particle multiplicity is expected to be small (of O(1)) for most of the Standard Model events while in various scenarios beyond the Standard Model.

Several physics scenarios predicting the presence of new extra low-mass weakly coupled particles, are accessible to PADME.

- *Dark photons:* Dark photons are produced through the process $e^+ + e^- \to \gamma + A'$. The detection strategy depends on the faith of A'. In the case of long lived or invisibly decaying A' the quantity of interest is the missing mass M_{miss}, with the recoil γ being measured by the calorimeter. In the case of (quasi) prompt $A' \to e^+e^-$ decays the electron and the positron would be detected by the charged particle detectors and can further be used to suppress the background. In addition, e^+/e^- momentum determination would provide extra information on the event kinematics.

  In the case of resonant or A'-strahlung production the discriminating quantity is the presence of an electron-positron pair with a given invariant mass. However this scenario may require more advanced tracking and momentum measurement.

- *Axion like particles:* The production machanism of ALPs can be very similar to the dark photon [22]. Depending on the couplings between the ALP a and the photon and the APL and the electron one may expect either direct annihilation into $a + \gamma$ or so called Primakoff production through $e^+e^- \to \gamma^* \to a + \gamma$.

  The search strategy is similar to the dark photon. In the case of ALP decaying into two photons, a di-photon invariant mass search could be performed. A requirement for the presence of a third photon will further decrease the background contribution.

- *New light scalars:* The dark photon A' can acquire mass through an interaction with an extra light scalar h', similar to the Higgs mechanism of the Standard Model [60]. The coupling between h' and A' is not suppressed by the small ϵ. In the region of the parameter space where A' is light and the mass of h' satisfies $M_{h'} > 2M_{A'}$, the h'-strahlung can take place and can lead to

$$e^+ + e^- \to \gamma^* \xrightarrow{\epsilon^2} A'^* \to A' + h' \to A' + A' + A' \to 3(e^+e^-). \tag{3}$$

  Such process will lead to striking multi-lepton final states. Despite its complexity, this process is a tree level process in the dark sector, while the corresponding Standard model is $\sim \alpha^6$, resulting in a very low cross-section.
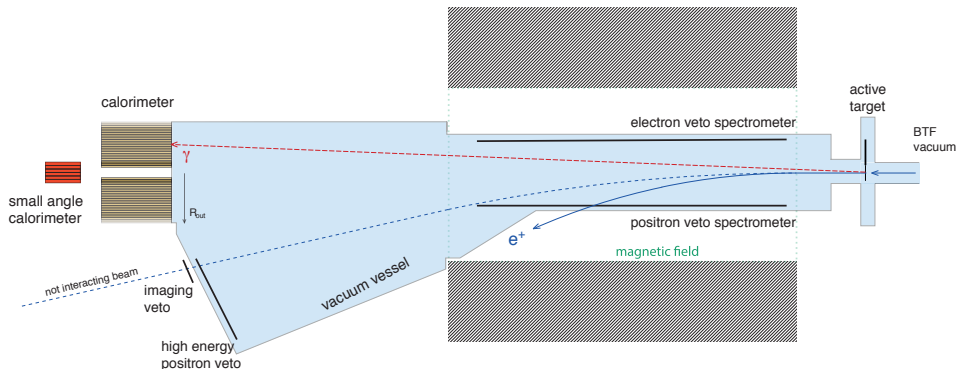
Figure 3: A schematics of the PADME experiment.

2.3.2. Present PADME setup

A sketch of the PADME experiment is shown in fig. 3. The beam is transported in vacuum through almost the whole setup. This is ensured by a large two-section vacuum chamber. The upstream section of the chamber, made by non magnetic stainless steal, is placed inside a dipole magnet which is able to provide 0.6 T magnetic field in a large volume. The downstream section geometry follows the deflected beam and also covers the acceptance of the PADME detectors.

PADME uses a 100 μm thick active diamond target with transversal dimensions of 20×20 mm^2 [61]. Horizontal and vertical 1 mm wide graphitic strips are used to extract the ionization signal from the traversing beam and to determine the bunch position and multiplicity. The final state photons are detected by the PADME calorimetric system. It consists of a quasi ring-shaped crystal calorimeter, composed by 616 assemblies of BGO inorganic crystal and an HZC XP1911 photomultipliers, the so-called ECal [62]. The central hole is covered by a Cherenkov calorimeter, the SAC, based on PbF$_2$ and Hamamatsu R13478UV photomultipliers [33]. The Cherenkov detector is able to withstand the high photon rate due to bremsstrahlung in the target while the ECal provides better energy resolution for photons in the range 50 MeV $< E_\gamma <$ 450 MeV. Three modules of segmented plastic scintillator detectors (PVeto, EVeto, HEPVeto) equipped with silicon photomultipliers and custom designed front-end electronics are located inside the vacuum chamber of the experiment [63]. They detect the positrons (electrons) with momentum in the approximate range 50 MeV$< E_{e+} <$450 MeV for the PVeto (EVeto) and 450 MeV$< E_{e+} <$500 MeV for the HEPVeto. Both the EVeto and PVeto are placed inside the magnetic field while the HEPVeto is close to the beam exit window.

PADME experiment also exploits two sets of silicon pixel detectors for beam monitoring - the Timepix and the MIMOSA. MIMOSA is occasionally placed instead of the active diamond target for beam tuning while the Timepix is located at the beam exit to measure the positions of the positrons in the bunch and is intended to be operational throughout the nominal data taking.

The DAQ system of PADME uses extensively the CAEN V1742 digitizer board which is based on the switched capacitor array DRS4 chip [64]. A single board hosts 32 ADC channels with 2 external trigger inputs, digitized together with the ADC channels to improve the timing. The maximal number of recorded samples is 1024, with Δt between two consequent samples of 200 ps, 400 ps and 1 ns (equivalent sampling frequency 5 GS/s, 2.5 GS/s and 1 GS/s, 1 ns maximal length of the recorded waveform). The dead time after a trigger is about 200 μs.

2.3.3. High statistics positron-on-target-annihilation perspectives

PADME took data with its nominal setup in the autumn/winter 2018/2019 (RUN I), two test runs in summer 2019 and 2020, and long physics run in the autumn, 2020 (RUN II).

All PADME runs utilized directly the DAΦNE Linac beam (either primary or secondary) with extended bunch length, varying from 100 ns up to about 320 ns. The Linac is able to provide 49 bunches of positrons

and electrons per second (bunch spacing of 20 ms). The maximal number of positrons, delivered to the PADME setup, is determined by the requirement to have about 100 e^+ per 1 ns. This rate, coupled to the sub-nanosecond time resolution of the PADME detectors ensures reliable event reconstruction and separation of close-in-time events. With the present PADME setup the bunch intensity is tuned to the optimal of about 25×10^3 positrons per bunch. The bunch length of the Linac cannot be extended to more than about 800 ns (see section 2.2) and to increase of the statistics significantly the running time has be increased.

An alternative to the direct Linac beam is to use a storage ring with addition extraction line. The present DAΦNE facility is a natural candidate, where two scenarios can be foreseen - the usage of the present positron ring or a of more simpler separate accumulator ring (see section 2.2 and refs. [41], [37]). The bunch length varies for the different extractions options, but is in the range of O(100 μs) to O(2 ns). The resonant extraction of the beam can lead to about $10^{16} - 10^{17}$ PoT per year, assuming extraction density of 100 positrons per ns.

2.3.4. Possible upgrades

To profit from the resonant beam extraction and the higher possible positron flux two types of upgrades of the PADME setup can be foreseen:

- *DAQ upgrade:* The present DAQ is switched capacitor based with a time-limited readout window window and non-negligible dead time. In addition, the current trigger signal originates from the Linac bunch signal. In the case of long length or continuous spill an event based triggering is necessary with possibly zero dead time. Such data acquisition can be achieved by Flash-ADC readout. An event-based trigger with preliminary cluster reconstruction could reduce the trigger rate significantly. The experience from running PADME experiment indicate that a uniform DAQ solution is preferred - even the channels which are not subject to be included in the generation of the trigger signal should share the same DAQ architecture. This will allow to reduce the development time and the subsequent maintenance efforts. Expected cost of the system is O(500 euro) per channel.

- *Detector upgrade:* To profit from the higher event rate an optimization of the time resolution of the different detectors can be performed. The addition of a second SiPM readout for the PVeto and the EVeto could lead to O(500 ps) time resolution for the electrons and positrons. This option is straight forward and is foreseen in the mechanical design of the two detectors.

  Another possibility to upgrade the PADME detector is the substitution of the BGO calorimeter with a faster inorganic scintillator calorimeter, for example LSO/LYSO, which exhibit O(40 ns) light decay time and allows better double pulse separation and shorter DAQ readout window, matching the EVeto and the PVeto one.

  A third option is the addition of a tracking system based on silicon pixel detectors close to the target. The tracker will allow precise vertex reconstruction and increased sensitivity to events with leptons in the final state and/or displaced vertex.

While the DAQ upgrade is unavoidable due to different beam extraction chain, the detector upgrade is subject to a compromise between performance and cost. Assuming the present PADME level of background contribution and an upgraded DAQ chain, a sensitivity to ϵ^2 down to 10^{-8} can be expected for the resonant beam extraction scenario. In the case of single positron reconstruction (possible in the so-called ultra-slow extraction), the background contribution will be negligible and sensitivity to ϵ^2 could be down to $10^{-9} - 10^{-10}$. These numbers are extrapolated from the nominal PADME sensitivity study and are preliminary. Advanced analysis techniques, including artificial intelligence methods (e.g. machine learning) both at the reconstruction stage and at the event selection stage, may further improve the experiment sensitivity.

2.4. Standard Model tests with positron beams (Isabella Oceano)

The PADME experiment made use, during 2019-2020 (Run II), of a bunched beam with an energy $E_{beam} \simeq 450$ MeV. Each bunch contained $\sim 28 \times 10^3$ positron hitting the diamond target (POT). In this

section we estimate production rates, and when possible visible rates, for SM processes assuming that in any future experiment the target will still be 100μm of Carbon. As benchmark scenario, we use Run II intensity conditions. Results for any different condition can be obtained scaling for the total number of POTs and target thickness.

Different SM final states originating from e^+e^- interactions can be investigated:

- final states with only photons: $e^+e^- \to \gamma\gamma(\gamma)$

- final states with only leptons: $e^+e^- \to e^+e^-$, $e^+e^- \to 2(e^+e^-)$, $e^+e^- \to 3(e^+e^-)$

- final states with a combination of both leptons and photons: $e^+e^- \to e^+e^-\gamma$, $e^+N \to e^+N\gamma$

2.4.1. Photon-only final states

The dominant processes with only photons are the annihilation to two or three photons ($e^+e^- \to \gamma\gamma(\gamma)$). These kind of events can be reconstructed by using the electromagnetic calorimeter (ECal) only. The leading order cross section of the annihilation $e^+e^+ \to \gamma\gamma$ is given by the Heitler formula:

$$\sigma(E, Z) = \frac{Z\pi r_e^2}{\gamma + 1} \times \left[\frac{\gamma^2 + 4\gamma + 1}{\gamma^2 - 1} ln\left(\gamma + \sqrt{\gamma^2 - 1}\right) - \frac{\gamma + 3}{\sqrt{\gamma^2 - 1}} \right] \tag{4}$$

where E is the positron energy, r_e is the classical electron radius and γ is the Lorentz factor of the beam particle.

The leading order cross section for a beam energy of $E_{beam} = 550$ MeV obtained with Eq. 4 is in agreement with CalcHEP [65] calculation: $\sigma(e^+e^- \to \gamma\gamma) = 1.55$ mb. In PADME, two photons in the ECal angular acceptance are required for the full reconstruction of these events. Using CalcHEP generated events, in the MC simulation of the experiment, the geometrical acceptance α and the efficiency ϵ of the event reconstruction have been calculated to be of the order of $\alpha \times \epsilon = 0.08$. In Tab. 3 estimations of the annihilation yield and the fully reconstructed events per day are provided.

To calculate the cross section of the three-photon final state precisely, the proper radiative corrections of the two photons process have to be evaluated. A raw estimate of the cross section can however be in any case extracted using the CalcHEP tool with a minimum photon energy cut to control the infrared divergence. We obtain 170 μb for $E_\gamma > 1$ MeV. A reliable value of detector acceptance is not easy to obtain without a proper generator, thus the yield of three-photon annihilation process is not yet precisely determined in PADME. An estimate of the order of magnitude obtained with CalcHEP calculation using $E_\gamma > 50$ MeV gives ~ 10 μb. In table 3 the number of events expected at PADME are reported. Due to the high instantaneous rate at PADME, these estimates are based only on the analysis of ECal signals, since the SAC calorimeter is overwhelmed by the Bremsstrahlung photons. A considerable increase in acceptance is expected using both the calorimeters in the analysis. In these conditions the main sources of background, as well as the luminosity uncertainty and reconstruction errors (few percent), would be strongly reduced. No cross section measurements exist for these processes at $\sqrt{s} \sim 20$ MeV, allowing PADME to measure them for the first time. With an error of $1 - 2\%$ on the cross section values, PADME aims to provide a significant comparison of the measurements with the Next Leading Order (NLO) calculation.

2.4.2. Final states with leptons and photons

The dominant processes with leptons and photons in the final states are Bremsstrahlung and radiative Bhabha. The Bremsstrahlung cross section at leading order was extracted using GEANT4 [66] and turned out to be of the order of $\sigma(e^+N \to e^+N\gamma) \simeq 4$ b, in the $E_{beam} = 550$ MeV hypothesis. Given that Bremsstrahlung photons are produced in the forward direction, PADME is expected to detect all of this radiation, with a geometrical acceptance very close to 1. In PADME, these events are reconstructed using the scintillating bars Positron Veto (PVeto) detector to detect the positron, and the SAC to detect the photon. In PADME Run II running conditions, the SAC occupancy was very high, and the reconstruction efficiency was reduced by the pileup. It is however possible to reconstruct the Bremsstrahlung yield relying only on the PVeto detector using a background-only (no target) run. Once calibrated, the Bremsstrahlung

yield can be used as a luminosity monitor for the experiment. This measurement can be compared with the other luminosity measurements in order to decrease their uncertainty and evaluate systematics. In PADME an excellent knowledge of this process is mandatory, since a positron veto inefficiency would mimic the dark photon signature, increasing the missing mass background.

The leading order radiative Bhabha $e^+e^- \to e^+e^-\gamma$ cross section is obtained by a CalcHEP calculation to be $\simeq 180$ mb for $E_{\gamma,e^+,e^-} > 1$ MeV.

To reproduce the experimental acceptance conditions, $E_\gamma > 50$ MeV and $E_{e^+,e^-} > 50$ MeV, the calculation was performed again including these cuts. We obtained a cross section value of $\simeq 0.131$ mb. PADME could be the first experiment to measure this cross section at $\sqrt{s} \sim 20$ MeV and compare it to the leading order calculation.

If a $X17$ particle exists it could manifest in PADME in final states like $e^+e^-\gamma$. If the radiative Bhabha kinematics is well understood, PADME can study the deviation from SM expectations and use the kinematics to try to identify the $X17$ particle. In PADME Run II running conditions this process is not easy to identify, but due to its relatively high cross section, it could be detected in a dedicated low intensity run.

2.4.3. Final state with leptons only

This category of events contains the Bhabha scattering and four- or six-lepton production. In order to identify multi-lepton final states, the signals of the PADME veto detectors are used on both the positron and electron (EVeto) sides of the sweeping magnet, requiring one or more pairs of in-time hits. The Bhabha scattering process is well known considering that it has been used as a luminosity monitor at e^+e^- colliders for decades. Much less is known about this process when the electrons are bounded to the nuclei of a fixed target especially if the impinging particle has low energy. The Bhabha cross section, calculated at leading order, is $\sigma(e^+e^- \to e^+e^-) \simeq 0.5$ b for a minimum electron energy of 1 MeV.

The PADME veto system is designed to detect positrons and electrons with an energy higher than an energy threshold of 50 MeV, reducing the visible cross section to $\simeq 3.3 \times 10^{-3}$ b. Due to high pileup and beam background, in PADME the observation of this process could be challenging. In a future scenario, with a continuous low density beam, the Bhabha scattering could be studied in detail also addressing possible resonant production of $X17$ boson in the process $e^+e^- \to X17 \to e^+e^-$.

Events with more than one pair of leptons in the final state, with four and six leptons, originate from gamma-gamma scattering:

$$e^+e^- \to e^+e^- X \qquad X \to e^+e^- \quad or \quad X \to e^+e^-e^+e^- \tag{5}$$

These processes are hard to be calculated in the SM, even at tree level, due to the large number of Feynman diagrams. Their detection in PADME Run II data is challenging due to the low average particle momentum compared to the PADME veto momentum threshold.

Concerning the four leptons, a semi analytical calculation was obtained by [67], and has been recently cross-checked with numerical calculation in [68]. The original leading log approximation

$$\sigma(e^+e^- \to 2(e^+e^-)) \approx \frac{28\alpha^4}{27\pi m_e^2}\left(log\frac{s}{m_e^2}\right)^3 \tag{6}$$

where s is the center of mass energy, has been demonstrated to be inadequate at the low energy relevant for the Frascati beams. Due to accidental cancellations at low energy, all the logarithmic terms need to be included, so that the cross section becomes:

$$\sigma(e^+e^- \to 2(e^+e^-)) \approx \frac{28\alpha^4}{27\pi m_e^2}\left[\left(log\frac{s}{m_e^2}\right)^3 - A\left(log\frac{s}{m_e^2}\right)^2 + B\left(log\frac{s}{m_e^2}\right) + C\right] + O\left(\frac{1}{s}\right) \tag{7}$$

where the constant terms are calculated in [67], and correspond to $A \simeq 6.36$, $B \simeq -11$ and $C \simeq 100$.

The result provided by equation Eq. (7) is in agreement with the CalcHEP [68], while Eq. Eq. (6) leads to a gross overestimate of the actual cross section. No cross section measurements exist for this process, and PADME could be the first experiment to check the theoretical predictions. In Tab. 3 the number of

14

Process	σ [pb]	N/$1E11$**POT**	$\sigma*$ [pb]	N*/$1E11$**POT**	tool used
$e^+e^- \to \gamma\gamma$	$1.55E9$	$1.8E6$	$0.12E9$	$1.3E5$	CalcHEP
$e^+e^- \to \gamma\gamma\gamma$	$0.170E9$	$1.9E5$	$0.01E9$	$1.2E4$	CalcHEP
$e^+N \to e^+N\gamma$	$4E12$	$4.7E9$	$4E12$	$\simeq 1E9$	Geant4
$e^+e^- \to e^+e^-\gamma$	$0.18E12$	$2.1E8$	$0.131E9$	$1.5E5$	CalcHEP
$e^+e^- \to e^+e^-$	$0.5E12$	$5.8E8$	$3.3E9$	$3.4E6$	CalcHEP
$e^+e^- \to 2(e^+e^-)$	$1.2E8$	1.4×10^5	$< 1.2E6$	$< 1.4E3$	CalcHEP
$e^+e^- \to 3(e^+e^-)$	$1.5E3$	2	not known	not known	/

Table 3: Cross sections and production rates of SM processes in PADME with standard Run II conditions, $E_{beam} \simeq 500$ MeV and $\simeq 28 \times 10^3$ POT/bunch, in a single day, $N_{POT} = 1.11 \times 10^{11}$. Cross sections and number of visible events in case the acceptance is known ($\sigma*$,N*).

four lepton events produced in a day using the standard PADME Run II conditions are indicated, while the acceptance is not yet known but it is expected to be <1%.

For $e^+e^- \to 3(e^+e^-)$, the calculation is too complex due to the huge number of Feynman diagrams and numerical calculations using both CalcHEP and MadGraph, failed. As in the case of four leptons, the cross section can be extracted using leading log EPA approximations [67].

$$\sigma(e^+e^- \to 3(e^+e^-)) = \frac{\alpha^2}{6\pi^2}\sigma(\gamma\gamma \to 2(e^+e^-))\left(log\frac{s}{m_e^2}\right)^4. \tag{8}$$

As in the previous case, the result is expected to be a gross over-approximation of the actual cross section value. Authors of [68] have developed a complete semi analytical formula, calculating the coefficients for the remaining logarithmic terms:

$$\sigma(e^+e^- \to 3(e^+e^-)) = \frac{\alpha^2}{6\pi^2}\sigma(\gamma\gamma \to 2(e^+e^-))\left[\left(log\frac{s}{m_e^2}\right)^4 + A\left(log\frac{s}{m_e^2}\right)^3 + B\left(log\frac{s}{m_e^2}\right)^2 + C\left(log\frac{s}{m_e^2}\right) + D\right]$$
$$\tag{9}$$

The two approximations show a high discrepancy [68], moreover Eq. 9 provides a cross section ∼10 times smaller than Eq. 8. The reduced SM expectation for this final state is extremely relevant, because this process is the main background to dark Higgs searches in the channel $e^+e^- \to A'h' \to (e^+e^- \to 3(e^+e^-))$. In Table 3 the number of the $e^+e^- \to 3(e^+e^-)$ events that can be produced at PADME are reported. In the case of six tracks with a total energy of 450 MeV, as in the PADME Run II, the probability that all six tracks have momentum above the threshold and within the PADME energy acceptance ($E > 50$ MeV) is very low. Therefore we do not expect to be able to observe this final state at PADME. In future, taking data with continuous beam and reduced magnetic field, could increase the luminosity and the acceptance allowing the experiment to precisely measure the $e^+e^- \to 3(e^+e^-)$ cross section and to search for dark sector final states.

2.4.4. Conclusion

Many SM processes can be investigated at PADME, either as by-product of the standard dark sector running conditions, or with dedicated runs. No measurements either at or close to the center of mass energy accessible at PADME exist for any of the described processes, thus PADME has the chance to be the first to perform some of these searches using the Run II data set. The precision reached in Run II data will be limited to a few % by the systematic errors on the luminosity measurement, despite a smaller statistical error. In a future scenario with a stretched beam delivering $10^{14} - 10^{16}$ POT/y [37], a PADME-like experiment could measure all the described processes with very high statistics and <1 % precision, testing NLO calculations and eventually beyond the SM contributions. An effort to compute part of these cross sections at NLO and to extract proper final state dynamics for simulations is already started using Baba Yaga [69] MC.

2.5. Potential reach for Dark Photons & ALP invisible searches with improved e^+ beams (Luc Darmé)

Among the various Feebly Interacting Particles (FIPs) candidates, ALPs and dark photons play a particularly important role. The former as it can be easily motivated by the presence of approximate symmetries in UV theories above the electroweak scale, and the latter as it a represents key ingredient in the phenomenology of very well-motivated models of sub-GeV dark matter as discussed in Sec. 2.1. Building on Sec. 2.2 and Sec. 2.3, we present in this section two positron-based experimental strategies to probe the invisible decay of such FIPs. In both cases, the –relatively– low energy of the available beam *does not constitute a drawback to probe new and theoretically-relevant parameter space.*

Production rates for FIPs at LNF. FIPs production rates in a positron-based machine are peculiar in that they have only a small dependence on the available energy of the incoming positron. Indeed, the available beam energy will determine not as much the expected FIPs production rates as the range of masses which can be probed. This range extends around the so-called resonant mass describing the precise mass of a FIP produced directly via resonant $e^+e^- \to X$:

$$M_{\rm res} = \sqrt{2E_+ m_e} \, , \tag{10}$$

where we wrote E_+ the energy of the incoming positron beam. While the FIP production rates are tremendously enhanced for this precise mass, it is clear that probing a significant mass range requires a mechanism to produce FIP at masses larger or smaller than the resonant one. The two relevant strategies are: (1) search for the higher order process $e^+e^- \to X\gamma$ (current PADME approach) or (2) use the natural energy attenuation of a positron beam in a semi-thick target to scan a range of resonant masses by effectively varying E_+ in Eq. (10). In both cases the relatively low energy of the available beam does not constitute a serious impediment but rather fix a unique window in the ten of MeV range where new physics scenarios may be probed to a staggering precision. We will briefly described both approaches below.

Mono-photon search: PADME+. Signal events rely on the process $e^+e^- \to X\gamma$ with the subsequent reconstruction of the photon allowing to probe the missing invariant mass. We use as a baseline scenario a $4 \cdot 10^{16}$ positron-on-target dataset, delivered by a POSEYDON-like beam line [31, 35, 37, 70] on an experiment similar to PADME. Based on the return of the currently-running PADME experiment, background control is a key requirement. We will assume that despite the significantly larger positron-on-target dataset, the number of background events will remain comparable with the current PADME run.

Missing energy: PADME-ME. Signal events rely on the process $e^+e^- \to X$ and trigger on missing energy/momentum for each individual incoming positron. In order to estimate the production rates in such a setup, we assume the presence of a high-Z, semi-thick target of $1/2$ radiation length. All events are required to have $E_{\rm th} = 200$ MeV of missing energy (corresponding to a bit less than half of the total incoming positron energy, chosen at $E_+ = 510$ MeV). The energy threshold determines the lowest accessible mass as $\sqrt{2E_{\rm th}m_e}$, although this lower limit may be mitigated in setups with large width FIP and by additional FIP production mechanisms. In order to trigger on the presence of missing energy, the beam should impact the target on a positron-per-positron basis. We hence use a baseline scenario of a 10^{14} positron-on-target dataset [70], broadly in line with the projection shown in Sec. 2.2.

Results. We present in Fig. 4 the corresponding number of events lines for both approaches, showing both a 100 and 2.3 signal event line. We stress that such lines do not include by design an estimate of the background and should not be considered projective limits. The results are shown for the two well motivated FIP scenarios presented above: a dark photon mediator setup and an ALP coupling mostly to electrons. The former being a key ingredient in light dark matter scenarios, we have overlaid the corresponding relic density targets for two choices of dark matter masses.

In the relevant five year time frame considered here, the two already-funded experiments probing a similar parameter space are NA64 [74] and Belle-II [73]. The former is based on a secondary electron beam of 100 GeV from the CERN SPS. The collaboration has released missing-energy limits based on a
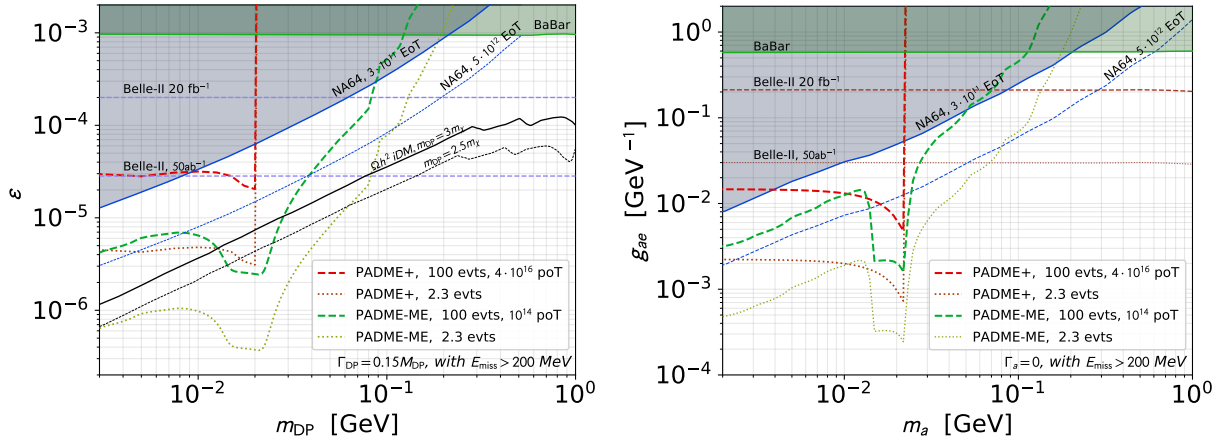
Figure 4: Number of expected signal events in a PADME+ or PADME-ME setup for (top) a dark photon model with a large width $\Gamma_{\rm DP} = 0.15 M_{\rm DP}$ and (bottom) an electrophilic ALP model with a zero width $\Gamma_a \sim 0$. In both cases, the thick dashed (resp. thin dotted) red line is the 100 (resp. 2.3) signal events line for a PADME+ setup while the thick dashed (resp. thin dotted) green line is the 100 (resp. 2.3) signal events line for a PADME-ME missing energy/momentum setup. For the missing mass setup, a missing energy of 200 MeV is required while the PADME+ scenario consider similar selection cuts as the current PADME experiment. The solid (dotted) blue line corresponds to the current (future) limit from NA64 [71]. The green region is the exclusion from mono-photon searches at BaBar [72]. The dashed (dotted) rust line gives the prospects at Belle-II [73] for a $20\,{\rm fb}^{-1}$ ($50\,{\rm ab}^{-1}$) dataset. For the dark photon case, the relic density targets are represented for an inelastic dark matter scenario with a dark matter mass m_χ satisfying $m_{\rm DP}/3$ (solid black line) and $m_{\rm DP}/2.5$ (dashed grey line).

2.84×10^{11} electron-on-target (EoT) dataset [75], with plan for 5×10^{12} EoT in the next years. We show a naive extrapolation based on this dataset, optimistic in that it assumes that NA64 will maintain a negligible background even with an order of magnitude increases in statistics. Belle-II is on the other hand a B-factory experiment which can probe FIPs based on mono-photon signatures. We show projective limits based on the collaboration projections [73], assuming an initial dataset of $20\,{\rm fb}^{-1}$ (twice the amount currently on tape). Although the total Belle-II planned dataset of $50\,{\rm ab}^{-1}$ will be much larger, achieving it will take around a decade.

It is clear from Fig. 4 that both experimental setup have the potential to probe new and physically relevant parameter space, with PADME-ME being more ambitious and potentially much more sensitive than PADME+. These results also illustrate the experimental challenges for both scenarios. In particular, a PADME+ proposal should aim at achieving a large background reduction by around 10^3 compared to the current PADME experiment, for instance via pile-up reduction and improved detector apparatus. In turn, the PADME-ME setup enjoys much larger FIP production rates, but rely heavily on a beam line setup delivering positron "individually" to ensure a very low background environment.

Finally, although we have shown in Fig. 4 and invisible FIP decay signatures, we stress that both PADME+ and PADME-ME can be used to search for additionally for visible FIP decays, for instance via $\gamma e^+ e^-$ or multileptons final states [68] for the former, or displaced vertices search for the latter.

Overall, we point out from this short analysis that the relatively low energy available does not constitute a limitation, but rather a strong incentive in searching for FIP in the tens of MeV regime. We strongly advocate for further studies focusing on the background estimates for both scenarios, in particular to determine if the lower energy environment may offer or not low background levels for a PADME-ME approach, and if the strong background reduction required in PADME+ compared to the current PADME experiment is feasible.

2.6. References

[1] G. Arcadi, M. Dutra, P. Ghosh, M. Lindner, Y. Mambrini, M. Pierre, S. Profumo, F. S. Queiroz, The waning of the WIMP? A review of models, searches, and constraints, Eur. Phys. J. C 78 (3) (2018) 203. `arXiv:1703.07364, doi:10.1140/epjc/s10052-018-5662-y`.

[2] J. L. Feng, et al., Planning the Future of U.S. Particle Physics (Snowmass 2013): Chapter 4: Cosmic Frontier, in: Community Summer Study 2013: Snowmass on the Mississippi, 2014. `arXiv:1401.6085`.

[3] J. L. Hewett, et al., Planning the Future of U.S. Particle Physics (Snowmass 2013): Chapter 2: Intensity Frontier, in: Community Summer Study 2013: Snowmass on the Mississippi, 2014. `arXiv:1401.6077`.

[4] J. Alexander, et al., Dark Sectors 2016 Workshop: Community Report, 2016. `arXiv:1608.08632`.

[5] M. Battaglieri, et al., US Cosmic Visions: New Ideas in Dark Matter 2017: Community Report, in: U.S. Cosmic Visions: New Ideas in Dark Matter, 2017. `arXiv:1707.04591`.

[6] J. Beacham, et al., Physics Beyond Colliders at CERN: Beyond the Standard Model Working Group Report, J. Phys. G 47 (1) (2020) 010501. `arXiv:1901.09966, doi:10.1088/1361-6471/ab4cd2`.

[7] P. Agrawal, et al., Feebly-Interacting Particles:FIPs 2020 Workshop Report (2 2021). `arXiv:2102.12143`.

[8] T. Blum, A. Denig, I. Logashenko, E. de Rafael, B. L. Roberts, T. Teubner, G. Venanzoni, The Muon (g-2) Theory Value: Present and Future (11 2013). `arXiv:1311.2198`.

[9] R. Pohl, et al., The size of the proton, Nature 466 (2010) 213–216. `doi:10.1038/nature09250`.

[10] C. E. Carlson, The Proton Radius Puzzle, Prog. Part. Nucl. Phys. 82 (2015) 59–77. `arXiv:1502.05314, doi:10.1016/j.ppnp.2015.01.002`.

[11] J. J. Krauth, et al., The proton radius puzzle, in: 52nd Rencontres de Moriond on EW Interactions and Unified Theories, 2017, pp. 95–102. `arXiv:1706.00696`.

[12] F. E. Wietfeldt, G. L. Greene, Colloquium: The neutron lifetime, Rev. Mod. Phys. 83 (4) (2011) 1173–1192. `doi:10.1103/RevModPhys.83.1173`.

[13] G. L. Greene, P. Geltenbort, The Neutron Enigma, Scientific American 314 (2016) 36–41. `doi:10.1038/scientificamerican0416-36`.

[14] L. Sbordone, P. Bonifacio, E. Caffau, H.-G. Ludwig, N. T. Behara, J. I. González Hernández, M. Steffen, R. Cayrel, B. Freytag, C. Van't Veer, et al., The metal-poor end of the spite plateau, Astronomy & Astrophysics 522 (2010) A26. `doi:10.1051/0004-6361/200913282`.
URL `http://dx.doi.org/10.1051/0004-6361/200913282`

[15] A. Krasznahorkay, et al., New experimental results for the 17 MeV particle created in ^8Be, EPJ Web Conf. 137 (2017) 08010. `doi:10.1051/epjconf/201713708010`.

[16] A. Krasznahorkay, et al., New evidence supporting the existence of the hypothetic X17 particle (10 2019). `arXiv:1910.10459`.

[17] 2020 Update of the European Strategy for Particle Physics, CERN Council, Geneva, 2020. `doi:10.17181/ESU2020`.

[18] E. Nardi, C. D. R. Carvajal, A. Ghoshal, D. Meloni, M. Raggi, Resonant production of dark photons in positron beam dump experiments, Phys. Rev. D 97 (9) (2018) 095004. `arXiv:1802.04756, doi:10.1103/PhysRevD.97.095004`.

[19] L. Marsicano, M. Battaglieri, M. Bondi', C. D. R. Carvajal, A. Celentano, M. De Napoli, R. De Vita, E. Nardi, M. Raggi, P. Valente, Dark photon production through positron annihilation in beam-dump experiments, Phys. Rev. D 98 (1) (2018) 015031. `arXiv:1802.03794, doi:10.1103/PhysRevD.98.015031`.

[20] L. Marsicano, M. Battaglieri, M. Bondí, C. D. R. Carvajal, A. Celentano, M. De Napoli, R. De Vita, E. Nardi, M. Raggi, P. Valente, Novel Way to Search for Light Dark Matter in Lepton Beam-Dump Experiments, Phys. Rev. Lett. 121 (4) (2018) 041802. `arXiv:1807.05884, doi:10.1103/PhysRevLett.121.041802`.

[21] A. Celentano, L. Darmé, L. Marsicano, E. Nardi, New production channels for light dark matter in hadronic showers, Phys. Rev. D 102 (7) (2020) 075026. `arXiv:2006.09419, doi:10.1103/PhysRevD.102.075026`.

[22] L. Darmé, F. Giacchino, E. Nardi, M. Raggi, Invisible decays of axion-like particles: constraints and prospects (12 2020). `arXiv:2012.07894`.

[23] P. Valente, B. Buonomo, L. Foggetta, Possible upgrades of the DAFNE Beam-Test Facility (BTF) (2014). `doi:10.15161/oar.it/1449018321.46`.

[24] P. Valente, et al., Linear Accelerator Test Facility at LNF: Conceptual Design Report (2016). `arXiv:1603.05651`.

[25] B. Wojtsekhowski, Searching for a U-boson with a positron beam, AIP Conf. Proc. 1160 (1) (2009) 149–154. `arXiv:0906.5265, doi:10.1063/1.3232023`.

[26] M. G. Pelizzo, et al., Optical components in harsh space environment, in: SPIE Optical Engineering + Applications, 2016, p. 99810G. `doi:10.1117/12.2237966`.

[27] B. Buonomo, C. Di Giulio, L. G. Foggetta, P. Valente, The Frascati LINAC Beam-Test Facility (BTF) Performance and Upgrades, in: 5th International Beam Instrumentation Conference, 2017, p. TUPG29. `doi:10.18429/JACoW-IBIC2016-TUPG29`.

[28] G. Chiodini, The PADME experiment, PoS EPS-HEP2019 (2020) 120. `doi:10.22323/1.364.0120`.

[29] A. Ghigo, et al., Commissioning of the DAFNE beam test facility, Nucl. Instrum. Meth. A 515 (2003) 524–542. `doi:10.1016/j.nima.2003.07.017`.

[30] B. Buonomo, L. G. Foggetta, G. Piermarini, New Gun Implementation and Performance of the DAΦNE LINAC, in: 6th International Particle Accelerator Conference, 2015, p. TUPWA056. `doi:10.18429/JACoW-IPAC2015-TUPWA056`.

[31] P. Valente, et al., Long beam pulses with SLED compression in DAΦNE LINAC, J. Phys. Conf. Ser. 874 (1) (2017) 012017. `doi:10.1088/1742-6596/874/1/012017`.

[32] M. Raggi, V. Kozhuharov, P. Valente, The PADME experiment at LNF, EPJ Web Conf. 96 (2015) 01025. `arXiv:1501.01867`, `doi:10.1051/epjconf/20159601025`.

[33] A. Frankenthal, et al., Characterization and performance of PADME's Cherenkov-based small-angle calorimeter, Nucl. Instrum. Meth. A 919 (2019) 89–97. `arXiv:1809.10840`, `doi:10.1016/j.nima.2018.12.035`.

[34] F. J. Decker, D. Farkas, L. Rinolfi, J. Truher, Reducing energy spread for long bunch train at SLAC, Conf. Proc. C 960610 (1996) 828–830.

[35] P. Valente, Ideas for extending the Frascati LINAC positron beam pulses for the resonant search of a X(17 MeV) boson (2020). `arXiv:2001.10258`.

[36] A. Fabris, et al., The LLRF System for the S-Band RF Plants of the FERMI Linac, IEEE Trans. Nucl. Sci. 63 (2) (2016) 861–868. `doi:10.1109/TNS.2015.2501649`.

[37] P. Valente, POSEYDON - Converting the DAΦNE Collider into a double Positron Facility: a High Duty-Cycle pulse stretcher and a storage ring (2017). `arXiv:1711.06877`.

[38] R. A. Beck, et al., Alis, an electron linac beam stretcher (project)., Conf. Proc. C 690827 (1969) 94–102.

[39] S. Guiducci, G. Martinelli, M. Preger, ALFA: Pulse Beam Stretcher for the Frascati Linac. Optical Structure and Performance Study, LNF-78/22-R (1978).

[40] L. O. Dallin, Operating Results of the Electron Ring of Saskatchewan (EROS), Conf. Proc. C 8903201 (1989) 22.

[41] S. Guiducci, et al., Proposal for Using DAΦNE as Pulse Stretcher for the Linac Positron Beam, J. Phys. Conf. Ser. 1067 (6) (2018) 062006. `doi:10.18429/JACoW-IPAC2018-THPAK023`.

[42] G. Benedetti, B. Buonomo, D. Filippetto, Emittance measurement of the DAΦNE LINAC electron beam, DAΦNE Technical Note LC-6 (2005).

[43] V. M. Biryukov, Y. A. Chesnokov, V. I. Kotov, Crystal channeling and its application at high-energy accelerators, 1997.

[44] A. Mazzolari, et al., Steering of a Sub-GeV Electron Beam through Planar Channeling Enhanced by Rechanneling, Phys. Rev. Lett. 112 (13) (2014) 135503. `doi:10.1103/PhysRevLett.112.135503`.

[45] S. Bellucci, et al., Using a deformed crystal for bending a sub-GeV positron beam, Nucl. Instrum. Meth. B 252 (2006) 3–6. `doi:10.1016/j.nimb.2006.04.058`.

[46] S. Bellucci, et al., Deflection of a 100-MeV positron beam by repeated reflections in thin crystals, JETP Lett. 98 (2014) 649–651. `doi:10.1134/S0021364013240041`.

[47] Y. Takabayashi, Y. L. Pivovarov, T. A. Tukhfatullin, Observation of sub-GeV electrons mirrored by ultrathin crystalline Si, Phys. Lett. B 751 (2015) 453–457. `doi:10.1016/j.physletb.2015.10.079`.

[48] M. Garattini, SHERPA: "Slow High-efficiency Extraction from Ring Positron Accelerator", LNF Seminar (2020).
URL https://agenda.infn.it/event/21911/

[49] V. Guidi, et al., Silicon crystal for channelling of negatively charged particles, Journal of Physics D: Applied Physics 42 (2009) 182005. `doi:10.1088/0022-3727/42/18/182005`.

[50] A. Sytov, et al., Planar channeling and quasichanneling oscillations in a bent crystal, The European Physical Journal C 76 (2015). `doi:10.1140/epjc/s10052-016-3923-1`.

[51] E. Bagli, et al., Steering efficiency of a ultrarelativistic proton beam in a thin bent crystal, Eur. Phys. J. C 74 (1) (2014) 2740. `arXiv:1311.4674`, `doi:10.1140/epjc/s10052-014-2740-7`.

[52] O. Blanco, M. Garattini, S. Guiducci, P. Valente, Studies of resonant and crystal-assisted positron extraction from DAΦNE rings, unpublished (2021).

[53] A. De Santis, DAΦNE status, 8th Low Emittance Rings Workshop (2020).
URL https://agenda.infn.it/event/20813/contributions/110188/

[54] S. Tomassini, et al., DAΦNE upgrade: A New magnetic and mechanical layout (2007) 1466–1468`doi:10.1109/PAC.2007.4440791`.

[55] L. O. Dallin, Time Controlled Monochromatic Extraction from EROS, in: 2nd European Particle Accelerator Conference (EPAC 90), 1990, p. 1260.

[56] M. E. Biagini, et al., Performance and operation of the DAPHNE accumulator, in: 6th European Particle Accelerator Conference (EPAC 98), 1998, pp. 415–417.

[57] M. Modena, H. Hsieh, C. Sanelli, High current density septum prototype for accumulator and storage rings of DAPHNE, the Frascati Phi factory, Conf. Proc. C 940627 (1995) 2403–2405.

[58] B. Bolli, et al., The Injection/Extraction 2 Degree Septum Magnets of the DAΦNE Accumulator, DAΦNE Technical Note MM-7 (1995).

[59] M. Raggi, V. Kozhuharov, Proposal to Search for a Dark Photon in Positron on Target Collisions at DAΦNE Linac, Adv. High Energy Phys. 2014 (2014) 959802. `arXiv:1403.3041`, `doi:10.1155/2014/959802`.

[60] B. Batell, M. Pospelov, A. Ritz, Multi-lepton Signatures of a Hidden Sector in Rare B Decays, Phys. Rev. D 83 (2011) 054005. `arXiv:0911.4938`, `doi:10.1103/PhysRevD.83.054005`.

[61] R. Assiro, et al., Performance of the diamond active target prototype for the PADME experiment at the DAΦNE BTF, Nucl. Instrum. Meth. A 898 (2018) 105–110. `arXiv:1709.07081`, `doi:10.1016/j.nima.2018.04.062`.

[62] P. Albicocco, et al., Characterisation and performance of the PADME electromagnetic calorimeter, JINST 15 (10) (2020) T10003. `arXiv:2007.14240`, `doi:10.1088/1748-0221/15/10/T10003`.

[63] F. Ferrarotto, L. Foggetta, G. Georgiev, P. Gianotti, V. Kozhuharov, E. Leonardi, G. Piperno, M. Raggi, C. Taruggi, L. Tsankov, P. Valente, Performance of the prototype of the charged-particle veto system of the padme experiment, IEEE Transactions on Nuclear Science 65 (8) (2018) 2029–2035. `doi:10.1109/TNS.2018.2822724`.

[64] E. Leonardi, M. Raggi, P. Valente, Development and test of a DRS4-based DAQ system for the PADME experiment at the DAΦNE BTF, J. Phys. Conf. Ser. 898 (3) (2017) 032024. `doi:10.1088/1742-6596/898/3/032024`.

[65] A. Belyaev, N. D. Christensen, A. Pukhov, Calchep 3.4 for collider physics within and beyond the standard model,

Computer Physics Communications 184 (7) (2013) 1729–1769. `doi:10.1016/j.cpc.2013.01.014`.
URL `http://dx.doi.org/10.1016/j.cpc.2013.01.014`

[66] S. Agostinelli, et al., Geant4—a simulation toolkit, Nuclear Instruments and Methods in Physics Research Section A: Accelerators, Spectrometers, Detectors and Associated Equipment 506 (3) (2003) 250–303. `doi:https://doi.org/10.1016/S0168-9002(03)01368-8`.
URL `https://www.sciencedirect.com/science/article/pii/S0168900203013688`

[67] V. Budnev, I. Ginzburg, G. Meledin, V. Serbo, The two-photon particle production mechanism. physical problems. applications. equivalent photon approximation, Physics Reports 15 (4) (1975) 181–282. `doi:https://doi.org/10.1016/0370-1573(75)90009-5`.
URL `https://www.sciencedirect.com/science/article/pii/0370157375900095`

[68] P. Ciafaloni, G. Martelli, M. Raggi, Searching for dark sectors in multi lepton final state in e+ e- collisions (12 2020). `arXiv:2012.04754`.

[69] C. M. Carloni Calame, G. Montagna, O. Nicrosini, F. Piccinini, The BABAYAGA event generator, Nucl. Phys. B Proc. Suppl. 131 (2004) 48–55. `arXiv:hep-ph/0312014`, `doi:10.1016/j.nuclphysbps.2004.02.008`.

[70] P. Valente, Options for improvements of the LNF e^+/e^- beam, Talk given at the meeting: *Fisica Fondamentale a Frascati*, LNF, 13 January 2021.
URL `https://agenda.infn.it/event/25299`

[71] D. Banerjee, et al., Search for Axionlike and Scalar Particles with the NA64 Experiment, Phys. Rev. Lett. 125 (8) (2020) 081801. `arXiv:2005.02710`, `doi:10.1103/PhysRevLett.125.081801`.

[72] J. P. Lees, et al., Search for Invisible Decays of a Dark Photon Produced in e^+e^- Collisions at BaBar, Phys. Rev. Lett. 119 (13) (2017) 131804. `arXiv:1702.03327`, `doi:10.1103/PhysRevLett.119.131804`.

[73] W. Altmannshofer, et al., The Belle II Physics Book, PTEP 2019 (12) (2019) 123C01, [Erratum: PTEP 2020, 029201 (2020)]. `arXiv:1808.10567`, `doi:10.1093/ptep/ptz106`.

[74] S. Andreas, et al., Proposal for an Experiment to Search for Light Dark Matter at the SPS (12 2013). `arXiv:1312.3309`.

[75] D. Banerjee, et al., Dark matter search in missing energy events with NA64, Phys. Rev. Lett. 123 (12) (2019) 121801. `arXiv:1906.00176`, `doi:10.1103/PhysRevLett.123.121801`.

3. Axion dark matter searches and Fundamental Physics with COLD-Lab

3.1. The theoretical allure of the QCD Axion (Enrico Nardi)

The non-trivial structure of the vacuum of Yang-Mills theories [1] implies that CP violation is a built-in feature in QCD [2, 3]. Strong CP violation is parametrized in terms of an angular variable $\theta \in [0, 2\pi]$ whose value is not determined by the theory, but is experimentally bounded to lie surprisingly close to zero $|\theta| \lesssim 10^{-10}$. It is hard to believe that this could simply occur as a whim of nature, especially because any value $\theta \lesssim 10^{-1}$ would leave our Universe basically unaffected [4–6] which precludes anthropic explanations. A convincing rationale for $\theta \approx 0$ is provided by the Peccei-Quinn (PQ) mechanism [7, 8], which postulates the existence of a global Abelian symmetry, endowed with a mixed $U(1)_{\rm PQ}$-$SU(3)_C$ anomaly and broken spontaneously. This unavoidably entails a quasi-massless spin zero boson, *the axion* [9, 10]. Remarkably, the axion also provides a novel solution to the apparently unrelated puzzle of the origin of dark matter (DM) [11–13], as well as a plethora of other implications for astrophysics and cosmology (for a recent review see [14]).

The customary shorthand description of how the axion 'solves the strong CP problem' is that it promotes the parameter θ to a dynamical quantity $\theta(x) = a(x)/f_a$ with $a(x)$ the axion field and f_a an effective mass scale. The axion potential has its minimum in $\theta(x) = 0$, and in this way the axion disposes of strong CP violation. While this is correct, I believe that it does not adequately convey how elegant and compelling the axion solution is. Let me then try to advocate its cogency by means of an analogy. Imagine the cabin of a boat that sails upwind with a steady angle of heel: everything is tilted, the floor, the table, the bunks. However, the hob is horizontal. An observer might conjecture that the hob was mounted not level by a drunk installer, and that the random installation angle is now matching accidentally the angle of heel. However, a careful measurement returns that the angle of inclination is bounded to be less than 10^{-10}. Then maybe there are 10^{10} sailing boats with hobs mounted at random angles, and only the observer on this boat will be able to cook, survive to destination, and report such a puzzling discovery. But, at a second thought, any hob with an angle smaller than 10^{-1} would work equally well, so why 10^{-10}? Eventually, the observer infers a convincing explanation: the hob is mounted on a gimbal that allows it to remain level when the boat is heeled. Gravity defines what is tilted and, with the help of the gimbal, gravity ensures that the hob will always remain level. In a similar way QCD levels out strong CP violation, with the help of the axion. The analogy can be pushed even further: when the boat starts heeling, any initial static friction in the gimbal would result in lifting slightly the hob center of mass, and if dynamical friction quickly drops to zero when the hob starts oscillating, imperceptible oscillations must still be going on. In the expanding Universe, 'Hubble friction' has precisely these properties, and the 'relic oscillations' that would prove the gimbal mechanism, are what axion dark matter searches with haloscopes are trying to detect.

The experimental sensitivity to oscillatory behaviours is greatly enhanced when resonant techniques, attempting to match the oscillator frequency, are employed. The sensitivity of resonant axion searches is well illustrated by Fig. 5, that shows how the limits on the axion-photon coupling set by haloscopes like ADMX and HAYSTAC are many order of magnitudes better than those of helioscopes like CAST. For the axion the oscillation frequency is given by its mass m_a. In benchmark axion models, when it is assumed that the PQ symmetry is broken after inflation, when only the contribution from the so-call *misalignment mechanism* described above is considered, and when it is assumed that this contribution saturates the local DM density, the axion mass is predicted to lie in a range between a few and several tenths of μeV. However, there is agreement that another contribution related to the decays of topological defects, which is unavoidably present in post-inflationary scenarios, is non-negligible, and some claim that it is the dominant one [15]. In this case the DM axion mass would lie at larger values (perhaps a bit anti-intuitively, the larger is m_a the smaller is the axion contribution to DM). In contrast, in pre-inflationary scenarios where the PQ symmetry is broken before inflation, and additional parameter contributes to determine the axion DM energy density (i.e. the initial value of θ) and the DM axion mass can easily lie below 1μeV (see [14] for a review of different possibilities). It goes without saying that it is extremely important to explore mass regions above and below the range suggested by the misalignment mechanism in a post-inflationary scenario. As is described in the next sections (and is resumed in Figs. 5 and 8) this is precisely the goal of the LNF axion search program with the QUAX-aγ experiment [16] and with the KLASH/FLASH [17, 18] large volume haloscope. If axions that lie in the corresponding mass windows are the dark matter, sooner or later they will be found.

3.2. QUAX-aγ: Search for the QCD axion with the LNF Haloscope (Claudio Gatti)

3.2.1. QUAX R&D

The QUAX (QUaerere AXion) experiment was proposed in 2017 as a modified haloscope containing magnetized media to detect galactic axions through their coupling to the electron spin [16]. In the same year, the CSN2 of INFN approved the QUAX R&D for a three-years period. The LNF group joined the groups of Padua and of the Laboratori Nazionali di Legnaro (LNL) in the project with the role of designing a resonant cavity with frequency of about 10 GHz and able to operate in a strong magnetic field while maintaining a quality factor larger than few 10^5. The Collaboration includes also the Salerno group, responsible for the design of the magnet, and the Trento-TIFPA group responsible for the superconducting electronics. The haloscope, put in operation at LNL, soon leaded to new limits both for the axions coupling to electrons [19, 20], the QUAXae experiment, and the coupling to photons [21, 22], the QUAXaγ experiment. The result in [21] was obtained with a NbTi resonant-cavity improving the quality factor by a factor 5 with respect to pure copper cavity when opearating in a magnetic field of about 6 Tesla [23]. With the latest result [22], shown in figure 5, the QUAX Collaboration reaches the sensitivity to QCD axions in the mass region around 40 μeV: this result is obtained by cooling down to 100 mK a copper cavity in a dilution refrigerator and amplifying the signal with a Josephson Parametric Amplifier (JPA) with a noise at the Standard Quantum Limit (SQL). We did further studies on dielectric resonant cavities [24, 25]. In
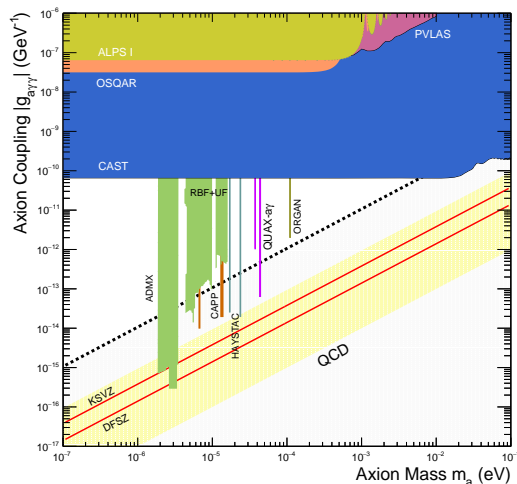
Figure 5: Exclusion limits for axions in the coupling-mass plane with recent QUAX-aγ results discussed in [22].

particular, we reached a quality factor of about 7×10^5 at 4 K with a cavity composed of two hollow sapphire cylinders, a value close to the limit imposed by the natural axion quality-factor $Q_a \sim 10^6$.

3.2.2. The LNF haloscope

In December 2019 we put in operation at the LNF COLD Laboratory [26] a dilution refrigerator, a Leiden CF-CS110-1000, with a Sumitomo pulse-tube with 1.5 W cooling power at 4.2 K, a base temperature of 8 mK and a mixing chamber plate of 490 mm diameter. The cooling power of the dilution refrigerator was measured to be 450 μW at 100 mK extendible up to 700 μW by improving the pumping capacity with a new turbo pump. The refrigerator is instrumented with four 0.86 mm BeCu-Ag-CuNi coaxial-lines thermalized at different temperatures down to the mixing chamber plate. The signal is read out through a fifth dedicated coaxial line connecting a sample holder at 10 mK, designed to host an amplifier or a single photon-device, to the HEMT amplifier mounted on the 4 K plate up to an SMA feedthrough on a 300 K flange. A standard setup for further amplification at room temperature, downconversion and digitization of
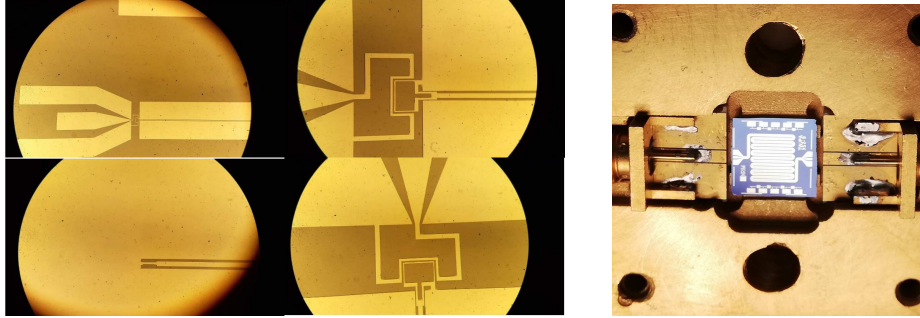
Figure 6: Left: optical image of the RF-chip with JJ and DC-SQUID fabricated at CNR-IFN for the SIMP project. Right: TWJPA from INRiM inside the LNF sample holder before bonding.

the signal was successfully tested during spring 2020. The delivery of a newly purchased 9 T magnet with 10 cm bore is expected for summer 2021.

In 2020, CSN5 of INFN approved the project DART WARS (Detector Array Readout with Traveling Wave AmplifieRS). Within this project we are testing Traveling Wave Josephson Parametric Amplifiers (TWJPA) chip fabricated at INRiM (right panel in Fig. 6). TWJPAs are based on a coplanar waveguide composed of an array of RF-SQUIDs [27]. The non-linearity of the inductance associated to the Josephson junctions gives rise to a mixing process that is exploited to transfer energy from a pump signal to a signal tone. The INRiM's implementation of this device, based on common Aluminum nano-fabrication technology, consists of a repetition of 990 elementary cells with a periodicity of 63 μm for a total length of about 6.25 cm. The device can operate both in a three-wave and in a four-wave mixing regimes with an expected amplification ranging from 25 to 35 dB in a bandwidth from 5 to 10 GHz depending on the operation mode. TWJPAs are used to readout arrays of qubits [28] coupled, through a readout cavity and a bandpass filter to a feedline terminated to a TWJPA for signal amplification in a 1.2 GHz wide band. A similar approach will be used in the LNF setup to read an array of resonant cavities hosted in the bore of the magnetic field as proposed in [29]. For a frequency of about 10 GHz up to 7 cavities, of diameter about 25 mm, can be hosted in a bore of 10 cm taking into account the thickness of cryostat radiation-shields and cavity walls.

Superconductive cavities will be employed to improve the quality factor. For NbTi cavity, already discussed in the previous section, a further improvement in quality factor is expected at few mK where the critical field reaches its maximum value of about 14 T. Superconductive YBCO cavity was measured at 7 GHz [30] showing a quality factor of about 330,000 in a 8 T magnetic field. Further tests are ongoing at LNF with YBCO and Nb3Sn.

In conclusion, the optimization of the magnetic volume together with the quantum-limited readout and superconductive cavities will allow the LNF haloscope to perform an axion search with a scan speed up to about 20 MHz per day.

Further improvements are expected by the development of single microwave photons detectors under study with the INFN funded project SIMP [31–34] and the H2020-FET project Supergalax [35]. Within the SIMP project, current biased Josephson Junctions (CBJJ) are tested at LNF as switching detector as described in [36]. We are currently testing at 10 mK chips fabricated at the CNR-IFN in Rome with Al transmission lines terminated by single JJ of DC-SQUID (left panel in Fig. 6) to determine their sensitivity to RF photons. These devices will also be operated and tested as JPAs. The Supergalax project is developing a single microwave photon counter based on an array of qubits exploting collective excitations to reduce the sensitivity to noise. These devices will be either directly coupled to the resonant cavity or connected with a coaxial line terminated through a proper impedance mathching circuit.

3.2.3. QUAX Experiment 2021-2025

In 2020 the CSN2 of INFN approved the plan to promote QUAX from the R&D to the experiment phase. The experiment will comprise two haloscopes one at LNL and one at LNF. The parameters for the two haloscopes are summarized in Table 4. We computed the scanning rates for the two systems for the

	LNF	LNL
Magnetic field	9 T	14 T
Magnet length	40 cm	50 cm
Magnet inner diameter	10 cm	12 cm
Frequency range	8.5 - 10 GHz	9.5 - 11 GHz
Cavity type	Hybrid SC	Dielectric
Scanning type	Inserted rod	Mobile cylinder
Number of cavities	7	1
Cavity length	0.3 m	0.4 m
Cavity diameter	25.5 mm	58 mm
Cavity mode	TM010	pseudoTM030
Single volume	$1.5 \cdot 10^{-4}$ m^3	$1.5 \cdot 10^{-4}$ m^3
Total volume	7⊗0.15 liters	0.15 liters
Q_0	300 000	1 000 000
Single scan bandwidth	630 kHz	30 kHz
Axion power	$7 \otimes 1.2 \cdot 10^{-23}$ W	$0.99 \cdot 10^{-22}$ W
Preamplifier	TWJPA/INRIM	DJJAA/Grenoble
Operating temperature	30 mK	30 mK
Performance for KSVZ model at 95% c.l. with $N_A = 0.5$		
Noise Temperature	0.43 K	0.5 K
Single scan time	3100 s	69 s
Scan speed	18 MHz/day	40 MHz/day
Performance for KSVZ model at 95% c.l. with $N_A = 1.5$		
Noise Temperature	0.86 K	1 K
Single scan time	12500 s	280 s
Scan speed	4.5 MHz/day	10 MHz/day

Table 4: Summary of the characteristics of the two QUAX Sikivie Haloscopes.

case of the KSVZ axion model with 95% c.l. Two different detector conditions have been considered, namely in the standard quantum limit ($N_A = 0.5$) and with extra noise added by the detection chain as $N_A = 1.5$ photons. For the LNF haloscope we assumed to operate the multicavity scheme in the simpler case with the cavities tuned at different frequencies. A successful operation of the cavities at the same frequency would improve the scanning rate by a further factor $N_{cav} = 7$. A realistic scan bandwidth of O(1) GHz is feasible for both set-ups, thus covering the yet unexplored region 8.5 to 11 GHz, corresponding to the axion mass range from 34 μeV to 44 μeV. Such physics reach is plotted in Fig. 7.
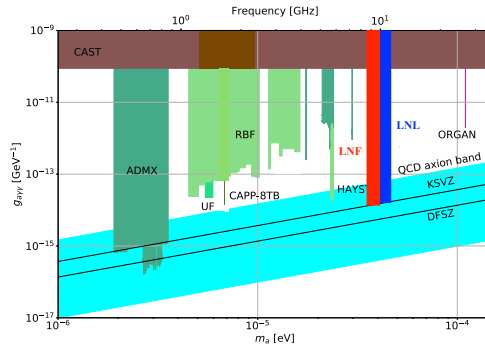

Figure 7: Expected physics reach for the QUAX-aγ experiment

With the LNL haloscope, having the best peak sensitivity, albeit over a much sharper band, some longer single runs can be envisaged. With such runs collected data should have sensitivity to reach the DFSZ model. We remind that the ratio of the expected axion power between DFSZ and KSVZ models is about 1/7.3. For the LNL haloscope this would mean increasing the single scan time from 69 s to about an hour.

Of course, if the collaboration will be able to operate a microwave quantum counter, all the performances will be boosted by a significant factor, depending on the noise rate of the detector. In such case, the studied bandwidth will essentially be limited by the operating bandwidth of the counter, and reaching the DFSZ model line will be a trustable goal.

3.3. From KLASH to FLASH. Search for axions with a Large Volume Haloscope (or: The art of recycling magnets) (Carlo Ligi)

In 2017, we wrote a proposal [17] for the realization of an haloscope devoted to the detection for sub-μeV axion at LNF. It was followed by a Letter of Intent and, in 2019, by a CDR [18]. The proposed experiment (KLASH, KLoe magnet for Axion SearcH) had the peculiarity of recycling the no longer used KLOE [37] magnet and the DAΦNE cryogenic plant, both at LNF. KLOE is a superconducting magnet with very large size bore, able to accommodate a cryogenic resonant cavity with a diameter of up to 3.7 m.

With the setup described in the CDR, it is possible to search for axion scanning in the frequency range 65-225 MHz, corresponding to axion masses between 0.3 and 1 μeV. As discussed in section 3.1, axion detection at the sub-μeV scale is a well motivated search.

On Tab. 5 the KLASH main calculated parameters are shown for the case of the axion's lowest detectable mass. Here, m_a is the axion mass, $g_{a\gamma\gamma}^{KSVZ}$ is the axion's coupling parameter of the KSVZ model, P_{sig} is the signal power, Rate is the expected axion's conversion frequency, B_{max} is the nominal KLOE magnetic field, β is the coupling between cavity and receiver, τ is the acquisition time, T_{sys} is the effective noise temperature of the system, $g_{a\gamma\gamma}$ is the expected axion-photon coupling for the considered m_a.

In Fig. 8 (left) we show the expected exclusion limits on $g_{a\gamma\gamma}$ for KLASH in the $0.3 - 1$ μeV mass range, compared with the expectations from the KSVZ and DFSZ models. Exclusion limits of other existing experiments are also highlighted.

Simulation shows that the quality factor Q for a copper cavity cooled at 4 K lies in the range $3 \div 7 \times 10^5$ in the considered frequency range. This implies that, in order to complete the frequency scan, a 3.5 years of integral data taking should be foreseen.

The cavity signal readout is based on a cryogenic amplification stage (a microstrip SQUID amplifier) followed by a room T readout chain which comprises an RF amplifier followed by an intermediate frequency mixer and a near audio frequency mixer stage, the last two arranged in a double-heterodyne receiver.

During the CDR writing, a preliminary study was carried out about the feasibility and the cost estimate of the realization and the installation of a liquid helium cryostat containing the copper cavity above mentioned. The cryostat has to be designed to fit and be inserted in KLOE magnet bore (Fig. 8 right), and should be equipped with a cryogenic turret which act as an interface with the cooling plant. The turret supplies the 4K liquid and 70K gaseous Helium to the cavity and the radiation shield, respectively.

In 2019 the collaboration was informed by INFN that the KLOE magnet would be destined for another experiment (DUNE). Following this decision, the collaboration considered the possibility to operate the FINUDA [38] magnet in its place. FINUDA is a superconducting solenoid similar to KLOE, placed on the DAΦNE hall at LNF and no longer in use since 2007. The differences respect to KLOE lie in the stronger magnet field (1.1 vs 0.6 T) and a smaller bore size (2.7 vs 4.8 m in diameter). From the axion sensitivity calculation point of view, these differences roughly compensate, so the expected signal power is very similar for both magnets. The frequency range will be higher than KLOE, due to the smaller dimension of the cavity.

The experiment proposal acronym is now FLASH (Finuda magnet for Light Axion SearcH).

Replacing the KLOE magnet with FINUDA implies a rewriting of the CDR and a new cost estimate study, due to several technical differences in the work to be done for adapting the magnet, in order to be used as an haloscope. KLOE is already placed in a building perfectly suitable to host the experiment, while FINUDA is

Figure 8: Left: the KLASH discovery potential compared to existing experimental limits. Right: a section view of the KLOE magnet surrounding the cryostat with its radiation shield and the copper cavity.

currently located in the DAΦNE hall. Two options are under investigation as where FLASH can be placed: either the present location, if it is possible to build a wall that can separate FINUDA from the DAΦNE main ring (which is likely to be working in the next few years), or moving FINUDA on the KLOE hall, after the KLOE magnet will be shipped in the USA. Moreover, the KLOE magnet worked perfectly for about 20 years until 2018, whereas FINUDA was energized last time in 2007, so the cryogenics and the power supply likely require a major refurbishment.

Taking in account on one side the smaller size of cavity and its cryostat, and so a reduction of their cost, and on the other side an increasing of other expenses for cryogenics and experiment hosting, we can affirm that the overall cost wouldn't be too much different with respect to the KLASH one. Nevertheless, some work is required to assure the magnet functionality, in terms of cryogenic stability and wire energization.

Table 5: Summary of KLASH parameter and discovery potential for KSVZ axions.

Parameter	Value
m_a [μeV]	0.27
$g_{a\gamma\gamma}^{KSVZ}$ [GeV^{-1}]	1.0×10^{-16}
P_{sig} [W]	1.33×10^{-22}
Rate [Hz]	3,050
B_{max} [T]	0.6
β	2
τ [min]	5
T_{sys} [K]	4.9
$g_{a\gamma\gamma}$ 90% c.l. [GeV^{-1}]	5.3×10^{-17}

3.4. Fundamental Physics with the LNF COLD-Lab (Danilo Babusci)

The quantum properties of the vacuum state constitute an area of quantum field theory that remains relatively unexplored experimentally. This can be traced to the extreme conditions under which the activity of the quantum vacuum become appreciable.

For this reason, researchers have turned the attention to analogue systems that are able to generate the desired amplification effects, and at the same time surmount the difficulties inherent in observations of the actual processes. Among this kind of systems, the superconducting devices play a special role.

In the following, we will concentrate our attention on the application of the TWJPA introduced in sec. 3.2 for demonstrating the analogous of the most amazing effect: the Hawking effect, i.e. the blackbody radiation supposed to be emitted at the horizon of a black hole [39, 40]. For an in-depth discussion of this and the other effects (parametric amplification, dynamical Casimir effect, Unruh effect) associated with the quantum vacuum, and the realization of their analogues by the superconducting devices, see Ref. [41].

The TWJPA can be modeled as a transmission line made of a series of capacitively shunted SQUIDs (or Josephson junctions) biased with an external magnetic flux that is allowed to vary with both position along the line and time. In the case in which the flux bias is represented by a step pulse whose front moves with speed u, as shown in Ref. [42], in the comoving frame of the propagating flux front, the equation of motion for the phase of the electromagnetic field along the line can be expressed in the 'general covariant' form:

$$\frac{1}{\sqrt{-g}} \partial_\mu \left(\sqrt{-g} g^{\mu\nu} \partial_\nu \varphi \right) = 0, \tag{11}$$

with $g = \det g_{\mu\nu}$ and the effective spacetime metric defined as

$$g^{\mu\nu} = \frac{1}{c(x)} \begin{pmatrix} -1 & u \\ u & c^2(x) - u^2 \end{pmatrix}. \tag{12}$$

where the speed $c(x)$ depends on the external flux bias Φ^{ext} and the constructive parameters of the device (the shunt capacity C_0, the cell length a, the critical current I_c of the SQUID junctions). This effective metric displays an event horizon ($g^{11} = g_{00} = 0$) where $c(x) = u$. As an example, let us consider a flux step of magnitude $\Phi^{\text{ext}} = 0.2 \, \Phi_0$ ($\Phi_0 = h/e$ is the quantum flux) with front that moves with speed $u = 0.95 \, c_0$ ($c_0 = c(x)|_{\Phi^{\text{ext}}=0}$), and where the flux bias is zero ahead of the propagating front (Fig. 9–top plot). The corresponding phase speed function is shown in the bottom plot of Fig. 9. By indicating with $x_h(t)$ the position for which $c(x_h, t) = u = 0.95 \, c_0$, well to the left of $x_h(t)$, electromagnetic waves travel with speed $0.9 \, c_0 < u$, while well to the right of $x_h(t)$, electromagnetic waves travel with speed $c_0 > u$. Thus the location $x_h(t)$ constitutes an effective moving event horizon.
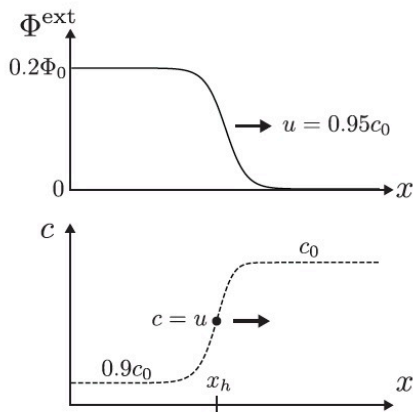
Figure 9: Propagating external flux bias step with front speed $u = 0.95 \, c_0$ (top plot) and the resulting electromagnetic wave phase speed in the SQUID array (bottom plot). The marked location $x_h(t)$ on the phase speed plot where $c(x_h, t) = u = 0.95 \, c_0$ constitutes an effective moving event horizon.

Assuming a propagating external flux bias step as described above, then photon pair production from the electromagnetic vacuum should occur in the vicinity of the event horizon, in direct analogy to Hawking radiation. The effective Hawking temperature is [43]

$$T_{\text{H}} = \frac{\hbar}{2\pi k_{\text{B}}} \left| \frac{\partial c(x)}{\partial x} \right|_{x_h}. \tag{13}$$

27

For example, for the phase speed step length about ten times the unit cell length a and a step height $0.1\,c_0$ as considered above, we have $|\partial c/\partial x|_{x_h} \approx 0.01\,c_0/a$, and thus [42]

$$T_{\mathrm{H}} \approx \frac{1}{100\pi k_{\mathrm{B}}} \sqrt{\frac{\hbar e I_c}{C_0}}, \tag{14}$$

that, for the realizable example circuit values $I_c = 5\,\mu\mathrm{A}$, $C_0 = 1\,\mathrm{fF}$ [44], gives $T_{\mathrm{H}} \approx 70\,\mathrm{mK}$.

An experimental run would require the repeated launching of propagating flux bias steps down the SQUID array, with the measured Hawking emitted photon pairs' correlation signal recovered through sufficiently long time-averaging along the lines of the acoustic Hawking radiation counterpart Bose-Einstein condensate experiment of Ref. [45]. In particular, for the above considered example parameter values, in the LAB frame, the emitted photon pairs propagate at speeds $0.9c_0$ and c_0 to the left and right of the moving event horizon, respectively, resulting in a spatial separation of the photon pairs and hence a delay in their arrival time at the photodetectors located at the right, terminal end of the SQUID array. Other, more sophisticated, detection methods, able to distinguish Hawking photon pairs from noise in a more unambigous way, are suggested in Ref. [42].

In conclusion, the ability to realize low noise, quantum limited microwave photon detectors, and SQUID arrays comprising thousands of unit cells operating at a few tens of mK temperatures and below [44], shows promise for demonstrating strong microwave Hawking radiation signals. At the same time, the full scope of quantum vacuum effects in superconducting circuits, and the possible applications thereof, is still unknown and need of further investigation.

3.5. References

[1] A. A. Belavin, A. M. Polyakov, A. S. Schwartz, Yu. S. Tyupkin, Pseudoparticle Solutions of the Yang-Mills Equations, Phys. Lett. B59 (1975) 85–87, [,350(1975)]. doi:10.1016/0370-2693(75)90163-X.

[2] C. G. Callan, Jr., R. F. Dashen, D. J. Gross, The Structure of the Gauge Theory Vacuum, Phys. Lett. B63 (1976) 334–340, [,357(1976)]. doi:10.1016/0370-2693(76)90277-X.

[3] R. Jackiw, C. Rebbi, Vacuum Periodicity in a Yang-Mills Quantum Theory, Phys. Rev. Lett. 37 (1976) 172–175, [,353(1976)]. doi:10.1103/PhysRevLett.37.172.

[4] L. Ubaldi, Effects of theta on the deuteron binding energy and the triple-alpha process, Phys. Rev. D81 (2010) 025011. arXiv:0811.1599, doi:10.1103/PhysRevD.81.025011.

[5] M. Dine, L. Stephenson Haskins, L. Ubaldi, D. Xu, Some Remarks on Anthropic Approaches to the Strong CP Problem, JHEP 05 (2018) 171. arXiv:1801.03466, doi:10.1007/JHEP05(2018)171.

[6] D. Lee, U.-G. Meißner, K. A. Olive, M. Shifman, T. Vonk, θ-dependence of light nuclei and nucleosynthesis, Phys. Rev. Res. 2 (3) (2020) 033392. arXiv:2006.12321, doi:10.1103/PhysRevResearch.2.033392.

[7] R. D. Peccei, H. R. Quinn, CP Conservation in the Presence of Instantons, Phys. Rev. Lett. 38 (1977) 1440–1443. doi:10.1103/PhysRevLett.38.1440.

[8] R. D. Peccei, H. R. Quinn, Constraints Imposed by CP Conservation in the Presence of Instantons, Phys. Rev. D16 (1977) 1791–1797. doi:10.1103/PhysRevD.16.1791.

[9] S. Weinberg, A New Light Boson?, Phys. Rev. Lett. 40 (1978) 223–226. doi:10.1103/PhysRevLett.40.223.

[10] F. Wilczek, Problem of Strong p and t Invariance in the Presence of Instantons, Phys. Rev. Lett. 40 (1978) 279–282. doi:10.1103/PhysRevLett.40.279.

[11] L. F. Abbott, P. Sikivie, A Cosmological Bound on the Invisible Axion, Phys. Lett. B120 (1983) 133–136. doi:10.1016/0370-2693(83)90638-X.

[12] M. Dine, W. Fischler, The Not So Harmless Axion, Phys. Lett. B120 (1983) 137–141. doi:10.1016/0370-2693(83)90639-1.

[13] J. Preskill, M. B. Wise, F. Wilczek, Cosmology of the Invisible Axion, Phys. Lett. B120 (1983) 127–132. doi:10.1016/0370-2693(83)90637-8.

[14] L. Di Luzio, M. Giannotti, E. Nardi, L. Visinelli, The landscape of QCD axion models, Phys. Rept. 870 (2020) 1–117. arXiv:2003.01100, doi:10.1016/j.physrep.2020.06.002.

[15] M. Gorghetto, E. Hardy, G. Villadoro, More Axions from Strings (7 2020). arXiv:2007.04990.

[16] R. Barbieri, C. Braggio, G. Carugno, C. S. Gallo, A. Lombardi, A. Ortolan, R. Pengo, G. Ruoso, C. C. Speake, Searching for galactic axions through magnetized media: the QUAX proposal, Phys. Dark Univ. 15 (2017) 135–141. arXiv:1606.02201, doi:10.1016/j.dark.2017.01.003.

[17] D. Alesini, et al., KLASH Conceptual Design Report (2019). arXiv:1911.02427.

[18] D. Alesini, et al., The klash proposal (2017). arXiv:1707.06010.

[19] N. Crescini, D. Alesini, C. Braggio, G. Carugno, D. Di Gioacchino, C. S. Gallo, U. Gambardella, C. Gatti, G. Iannone, G. Lamanna, C. Ligi, A. Lombardi, A. Ortolan, S. Pagano, R. Pengo, G. Ruoso, C. C. Speake, L. Taffarello, Operation of a ferromagnetic axion haloscope at $m_a = 58\,\mu ev$, The European Physical Journal C 78 (9) (2018) 703. doi:10.1140/epjc/s10052-018-6163-8.
URL https://doi.org/10.1140/epjc/s10052-018-6163-8

[20] N. Crescini, D. Alesini, C. Braggio, G. Carugno, D. D'Agostino, D. Di Gioacchino, P. Falferi, U. Gambardella, C. Gatti, G. Iannone, C. Ligi, A. Lombardi, A. Ortolan, R. Pengo, G. Ruoso, L. Taffarello, Axion search with a quantum-limited ferromagnetic haloscope, Phys. Rev. Lett. 124 (2020) 171801. doi:10.1103/PhysRevLett.124.171801.
URL https://link.aps.org/doi/10.1103/PhysRevLett.124.171801

[21] D. Alesini, C. Braggio, G. Carugno, N. Crescini, D. D'Agostino, D. Di Gioacchino, R. Di Vora, P. Falferi, S. Gallo, U. Gambardella, C. Gatti, G. Iannone, G. Lamanna, C. Ligi, A. Lombardi, R. Mezzena, A. Ortolan, R. Pengo, N. Pompeo, A. Rettaroli, G. Ruoso, E. Silva, C. C. Speake, L. Taffarello, S. Tocci, Galactic axions search with a superconducting resonant cavity, Phys. Rev. D 99 (2019) 101101. doi:10.1103/PhysRevD.99.101101.
URL https://link.aps.org/doi/10.1103/PhysRevD.99.101101

[22] QUAX Collaboration, arxiv:2012.09498 submitted to P.R.D.

[23] D. Di Gioacchino, C. Gatti, D. Alesini, C. Ligi, S. Tocci, A. Rettaroli, G. Carugno, N. Crescini, G. Ruoso, C. Braggio, P. Falferi, C. S. Gallo, U. Gambardella, G. Iannone, G. Lamanna, A. Lombardi, R. Mezzena, A. Ortolan, R. Pengo, E. Silva, N. Pompeo, Microwave losses in a dc magnetic field in superconducting cavities for axion studies, IEEE Transactions on Applied Superconductivity 29 (5) (2019) 1–5. doi:10.1109/TASC.2019.2897267.

[24] D. Alesini, C. Braggio, G. Carugno, N. Crescini, D. D'Agostino, D. Di Gioacchino, R. Di Vora, P. Falferi, U. Gambardella, C. Gatti, G. Iannone, C. Ligi, A. Lombardi, G. Maccarrone, A. Ortolan, R. Pengo, C. Pira, A. Rettaroli, G. Ruoso, L. Taffarello, S. Tocci, High quality factor photonic cavity for dark matter axion searches, Rev. Sci. Instrum. 91 (9) (2020) 094701. doi:10.1063/5.0003878.
URL https://doi.org/10.1063/5.0003878

[25] D. Alesini, C. Braggio, G. Carugno, N. Crescini, D. D'Agostino, D. Di Gioacchino, R. Di Vora, P. Falferi, U. Gambardella, C. Gatti, G. Iannone, C. Ligi, A. Lombardi, G. Maccarrone, A. Ortolan, R. Pengo, C. Pira, A. Rettaroli, G. Ruoso, L. Taffarello, S. Tocci, Realization of a high quality factor resonator with hollow dielectric cylinders for axion searches, Nucl. Instrum. Methods A 985 (2021) 164641. doi:https://doi.org/10.1016/j.nima.2020.164641.
URL http://www.sciencedirect.com/science/article/pii/S016890022031038X

[26] Cold lab, http://coldlab.lnf.infn.it.

[27] A. B. Zorin, Josephson traveling-wave parametric amplifier with three-wave mixing, Phys. Rev. Applied 6 (2016) 034006. doi:10.1103/PhysRevApplied.6.034006.
URL https://link.aps.org/doi/10.1103/PhysRevApplied.6.034006

[28] J. Heinsoo, C. K. Andersen, A. Remm, S. Krinner, T. Walter, Y. Salathé, S. Gasparinetti, J.-C. Besse, A. Potočnik, A. Wallraff, C. Eichler, Rapid high-fidelity multiplexed readout of superconducting qubits, Phys. Rev. Applied 10 (2018) 034040. doi:10.1103/PhysRevApplied.10.034040.
URL https://link.aps.org/doi/10.1103/PhysRevApplied.10.034040

[29] B. T. McAllister, G. Flower, E. N. Ivanov, M. Goryachev, J. Bourhill, M. E. Tobar, The organ experiment: An axion haloscope above 15 ghz, Physics of the Dark Universe 18 (2017) 67 – 72. doi:https://doi.org/10.1016/j.dark.2017.09.010.
URL http://www.sciencedirect.com/science/article/pii/S2212686417300602

[30] D. Ahn, O. Kwon, W. Chung, W. Jang, D. Lee, J. Lee, S. W. Youn, D. Youm, Y. K. Semertzidis, Superconducting cavity in a high magnetic field (2020). arXiv:2002.08769.

[31] D. Alesini, D. Babusci, C. Barone, B. Buonomo, M. M. Beretta, L. Bianchini, G. Castellano, F. Chiarello, D. D. Gioacchino, P. Falferi, G. Felici, G. Filatrella, L. G. Foggetta, A. Gallo, C. Gatti, F. Giazotto, G. Lamanna, F. Ligabue, N. Ligato, C. Ligi, G. Maccarrone, B. Margesin, F. Mattioli, E. Monticone, L. Oberto, S. Pagano, F. Paolucci, M. Rajteri, A. Rettaroli, L. Rolandi, P. Spagnolo, A. Toncelli, G. Torrioli, Development of a josephson junction based single photon microwave detector for axion detection experiments, Journal of Physics: Conference Series 1559 (2020) 012020. doi:10.1088/1742-6596/1559/1/012020.

[32] D. Alesini, D. Babusci, C. Barone, B. Buonomo, M. M. Beretta, L. Bianchini, G. Castellano, F. Chiarello, D. Di Gioacchino, P. Falferi, G. Felici, G. Filatrella, L. G. Foggetta, A. Gallo, C. Gatti, F. Giazotto, G. Lamanna, F. Ligabue, N. Ligato, C. Ligi, G. Maccarrone, B. Margesin, F. Mattioli, E. Monticone, L. Oberto, S. Pagano, F. Paolucci, M. Rajteri, A. Rettaroli, L. Rolandi, P. Spagnolo, A. Toncelli, G. Torrioli, Status of the simp project: Toward the single microwave photon detection, Journal of Low Temperature Physics 199 (1) (2020) 348–354. doi:10.1007/s10909-020-02381-x.
URL https://doi.org/10.1007/s10909-020-02381-x

[33] A. S. Piedjou Komnang, C. Guarcello, C. Barone, C. Gatti, S. Pagano, V. Pierro, A. Rettaroli, G. Filatrella, Analysis of Josephson junctions switching time distributions for the detection of single microwave photons, Chaos Solitons and Fractals: the interdisciplinary journal of Nonlinear Science142 (2021) 110496. doi:10.1016/j.chaos.2020.110496.

[34] F. Paolucci, et al., Development of highly sensitive nanoscale transition edge sensors for gigahertz astronomy and dark matter search, J. Appl. Phys. 128 (19) (2020) 194502. arXiv:2007.08320, doi:10.1063/5.0021996.

[35] Supergalax h2020-fetopen-2018-2019-2020-01, https://supergalax.eu.

[36] L. S. Kuzmin, A. S. Sobolev, C. Gatti, D. Di Gioacchino, N. Crescini, A. Gordeeva, E. Il'ichev, Single Photon Counter based on a Josephson Junction at 14 GHz for searching Galactic Axions, IEEE Trans. Appl. Supercond. 28 (7) (2018) 2400505. doi:10.1109/TASC.2018.2850019.

[37] P. Franzini, M. Moulson, The physics of daϕne and kloe, Annual Review of Nuclear and Particle Science 56 (1) (2006)

207–251. `doi:10.1146/annurev.nucl.56.080805.140459`.

[38] M. Bertani, et al., The finuda superconducting magnet at dafne, Nuclear Physics B - Proceedings Supplements 78 (1) (1999) 553–558. `doi:https://doi.org/10.1016/S0920-5632(99)00602-7`.

[39] S. W. Hawking, Black hole explosions, Nature 248 (1974) 30–31. `doi:10.1038/248030a0`.

[40] S. W. Hawking, Particle Creation by Black Holes, Commun. Math. Phys. 43 (1975) 199–220, [Erratum: Commun.Math.Phys. 46, 206 (1976)]. `doi:10.1007/BF02345020`.

[41] P. D. Nation, J. R. Johansson, M. P. Blencowe, F. Nori, Stimulating Uncertainty: Amplifying the Quantum Vacuum with Superconducting Circuits, Rev. Mod. Phys. 84 (2012) 1. `arXiv:1103.0835`, `doi:10.1103/RevModPhys.84.1`.

[42] M. P. Blencowe, H. Wang, Analogue Gravity on a Superconducting Chip, Phil. Trans. Roy. Soc. Lond. A 378 (2177) (2020) 20190224. `arXiv:2003.00382`, `doi:10.1098/rsta.2019.0224`.

[43] R. Schutzhold, W. G. Unruh, Hawking radiation in an electro-magnetic wave-guide?, Phys. Rev. Lett. 95 (2005) 031301. `arXiv:quant-ph/0408145`, `doi:10.1103/PhysRevLett.95.031301`.

[44] C. Macklin, et al., A near-quantum-limited Josephson traveling-wave parametric amplifier, Science 350 (2015) 307. `doi:10.1126/science.aaa8525`.

[45] J. R. Muñoz de Nova, K. Golubkov, V. I. Kolobov, J. Steinhauer, Observation of thermal Hawking radiation and its temperature in an analogue black hole, Nature 569 (7758) (2019) 688–691. `arXiv:1809.00913`, `doi:10.1038/s41586-019-1241-0`.

4. Strong interaction with strangeness at DAΦNE (*Catalina Curceanu, Carlo Guaraldo, Kristian Piscicchia, Diana Sirghi, Alessandro Scordo, Johann Zmeskal*)

4.1. Fundamental physics at the strangeness frontier at DAΦNE: a unique opportunity

The DAΦNE collider at INFN-LNF [1], [2] is a unique source of strangeness (kaons) in the world: it delivers a low-momentum (< 140 MeV/c) nearly monochromatic charged kaon "beam", generated by the decay of the ϕ resonance formed in the collisions of electrons and positrons. This beam is ideal for experimental studies of low-energy kaon-nucleon/nuclei interactions.

Huge advances in the development of fast spectroscopic X-ray detector systems, as well as the availability of the DAΦNE kaon beam, propelled an unprecedented progress in the field of strangeness studies with the DEAR [3] and the SIDDHARTA [4] [5] [6] experiments, which achieved the most precise measurement of kaonic hydrogen transitions to the fundamental level, and the first measurements of kaonic helium-3 and gaseous kaonic helium-4 transitions to the 2p level. The importance of these studies is also reflected by the number of citations of the papers: [4] has more than 300 citations, [6] more than 100 and several other papers have more than 50 [5], [7]. Presently, the SIDDHARTA-2 collaboration is performing the challenging kaonic deuterium measurement which, due to its difficulty, could not be performed till now. All these measurements provide necessary inputs and constraints to fundamental physics with strangeness, in particular to the theoretical models describing the strong interaction in the low-energy regime [8].

In the same time, the AMADEUS collaboration has performed unprecedented studies of kaon-nuclei interactions at low-energies [9–13], which delivered a wealth of new experimental data used for understanding low-energy QCD with strangeness, with important impact in astrophysics. DAΦNE confirmed to be a unique machine in the world where to perform fundamental physics measurements at the strangeness frontier.

A broad international community, growing on the backbone of the SIDDHARTA-2 collaboration, proposes a strategy for future fundamental physics measurements at the strangeness frontier at DAΦNE, which is supported by the EU STRONG-2020 Project (Grant Agreement n. 824093), both for the theoretical impact and development, as well as for new detector systems realisation, and from various international and national agencies. This community proposes a five years post-SIDDHARTA-2 scientific program for kaonic atoms and kaon-nuclei interactions measurements focused on:

- Selected light and heavy kaonic atoms transitions (KA1, KA2, KA3)

- Low-energy kaon-nucleon scattering processes (KN1)

- Low-energy kaon-nuclei interactions (KN2)

to be performed with a series of detector systems developed within the proponent community. These measurements were selected as results of discussions and optimizations within a broad international community of theoreticians and experimentalists working in various fields, going from particle and nuclear physics to astrophysics and foundations of physics. A possible schematic schedule of the proposed measurements is shown in the Gantt Chart (see Fig. 10), and is being discussed in the following sections.

Experiment	1st year					2nd year					3rd year					4th year					5th year				
KA1
KA2
KA3
KN1
KN2

Figure 10: Schematic Gantt Chart for Fundamental physics at the Strangeness Frontier at the DAΦNE Proposal: KA1 (see Sec. 4.2.1), KA2 (see Sec. 4.2.2), KA3 (see Sec. 4.2.3), KN1 (see Sec. 4.3.2), KN2 (see Sec. 4.3.3). Yellow: preparation phase. Blue: installation phase. Red: data taking.

The frontier strangeness studies, which we propose to be performed at DAΦNE in a strategic series of measurements campaign, have a strong impact on many sectors of fundamental physics (see Fig. 11), among which:

31

- *Strong interaction:* QCD theory of the strong interaction in the low-energy regime, [8] [14–16];

- *Astrophysics:* the Equation of State of Neutron stars [17–25];

- *Dark Matter:* dark matter within the Standard Model, the Strange Dark Matter [26];

- *Fundamental physics:* the measurement of the charged kaon mass, solution to "kaon mass puzzle" [27, 28];

- *Physics beyond the Standard Model (BSM):* measurements with extreme precision of kaonic atoms transitions, similar to the muonic atoms measurements, which triggered the proton radius puzzle and the BSM searches with exotic atoms [29, 30].
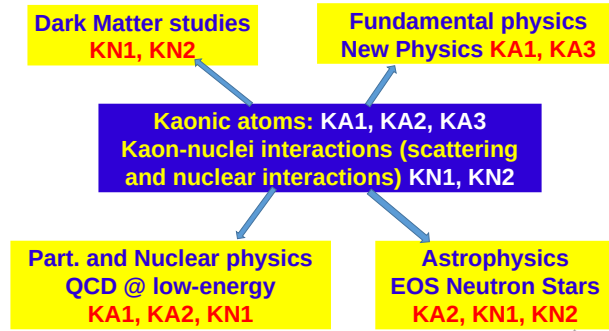
Figure 11: Impact of the Fundamental Physics at the Strangeness Frontier at DAΦNE studies.

We strongly believe that this is an opportunity which *cannot be missed*, since we propose to measure fundamental interaction processes which could not be measured till now, and which will have a huge and concrete impact, "now and here", in particle and nuclear physics, astrophysics, cosmology and foundational issues.

Our measurements have a huge potential of producing a consistent number of high-impact publications in high-impact factor journals, which will guide the developments of physics at strangeness frontier in the next 10-20 years, setting DAΦNE and LNF on the forefront of fundamental physics studies.

Note: *For details and recent discussions about the fundamental physics at the strangeness frontier, we refer to our dedicated workshop : "Fundamental physics at the strangeness frontier at DAΦNE", 25-26 February 2021, at : https://agenda.infn.it/event/25725/overview .*

4.2. Fundamental physics with kaonic atoms

Since the first kaonic hydrogen measurement performed by the DEAR collaboration [3], the strangeness physics international collaboration at DAΦNE has sensibly grown, not only in terms of number of participants and involved institutions but, also, in terms of expertize in technologies, such as cryogenic targets and detector systems, used for performing low-energy strangeness nuclear physics studies, in particular kaonic atoms measurements. The strong impact of the SIDDHARTA results, i.e., the kaonic hydrogen and helium measurements [4–6], and the expected SIDDHARTA-2 [7] kaonic deuterium one, together with the gathered experience and knowledge of our international community is the driving force of the series of future proposed experiments at the DAΦNE collider, having potential breakthrough impacts in several fields (see Sec. 4.1). We propose a series of kaonic atoms measurements, and briefly introduce the expected physics impact, the kaonic transitions to be measured, the required detector performances with a schematic setup and, finally, their feasibility and a first estimate of integrated luminosity requests.

4.2.1. Selected heavy kaonic atoms measurements (KA1)

- *Expected impact and physics motivation.* New precise measurements of heavy kaonic atoms transitions have a strong impact in two main directions shown in Sec. 4.1: the charged kaon mass puzzle [27][31] and QCD at low-energy, by the investigation of in-medium effects related to the multi-nucleon interaction of the kaons. In this direction, high-Z targets can be exploited to measure transitions both to low and high n levels, where in the first case results about multi-nucleon interaction can be obtained and in the second one, since high n levels transitions are purely QED, the charged kaon mass problem could be addressed. The KPb atom is, indeed, together with the KC one, *one of the two protagonists* of the charged kaon mass puzzle [27]. In all these experiments, the possibility to perform, for a single target, simultaneous measurements of atomic transitions from different n levels and with different Δn will also help in the systematic errors minimization and, in addition, provide useful information about the cascade process of heavy kaonic atoms [32].

- *Transitions to be measured.* We plan to perform a measurement campaign using Se, Zr, Ta and Pb targets; the lines to be measured are, $KSe(6, 5, 4 \rightarrow 5, 4, 3)$, $KZr(6, 5, 4 \rightarrow 5, 4, 3)$, $KTa(8, 7, 6 \rightarrow 7, 6, 5)$, $KPb(9, 8, 7, 6 \rightarrow 8, 7, 6, 5)$.

- *Detector performances and setup.* The above mentioned transitions cover a wide energy range spanning from few hundreds of keV up to few MeV. To measure with high precision these energies, we plan to implement a High Purity Germanium Detector (HPGe) which, thanks to a rate capability up to $150\,kHz$, could be positioned, with an appropriate shielding, close to the DAΦNE interaction point (IP) to maximize the geometrical efficiency. To test the in-beam behaviour and to assess the machine background effects on the system, an exploratory measurement is planned to be carried on in parallel with the SIDDHARTA-2 experiment. A sketch of the KA1 setup is show in Fig. 12 left, where the HPGe detector (e), the target (c) and its holder (d) are shown, together with part of the mechanical support and the lead shielding (f), the SIDDHARTA-2 luminosity monitor [33] to be used as trigger (b) and the DAΦNE beam pipe (a) [28].
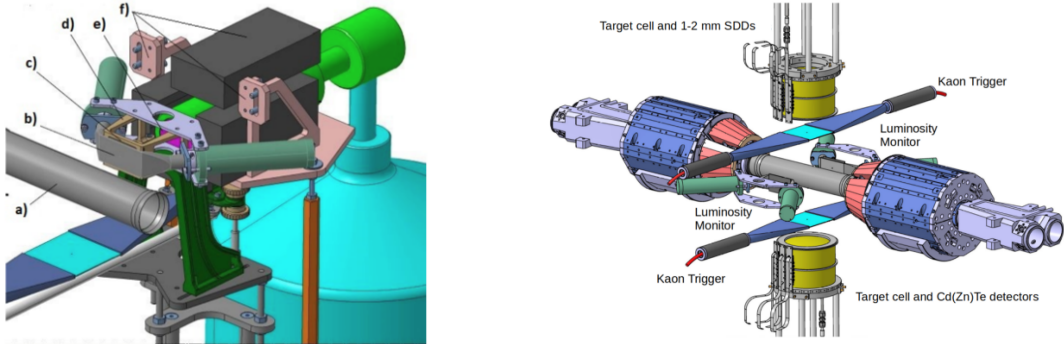

Figure 12: Setups of the KA1 (left) and KA2 (right) experiments (see text for details).

- *Luminosity request and feasibility.* The HPGe detector and its readout system have been already assembled at the University of Zagreb, where several tests confirmed its excellent performances in terms of energy resolution ($FWHM \simeq 1,12\,keV\,@\,300\,keV\,/\,1,17\,keV\,@\,1,3\,MeV$) and timing [28]. Assuming SIDDHARTA-like conditions ($\mathcal{L} = 1,4 \times 10^{32} \rightarrow 10\,pb^{-1}/day\,integrated$), from MC simulations we obtain that measurements with a precision of few eV could be achieved with a delivered integrated luminosity of $360\,pb^{-1}$ considering *the efficiency for each target*. These results can be obtained in an overall 8 months experiment: 2 months for the setup mounting and optimization and 6 months of data taking, if running with all four targets.

4.2.2. Selected light kaonic atoms measurements (KA2)

- *Expected impact and physics motivation.* Measurements of light kaonic atoms transitions are fundamental to address important open problems like kaon-nuclei potential and chiral models below threshold and the nature of the ambiguous $\Lambda(1405)$. These results are important also in astrophysics: search of dark matter with strangeness and the equation of state for neutrons stars [17–25]. In particular, the first ever measurement of the $K^{3,4}He(2p \rightarrow 1s)$ transition will put stronger constraints on the theoretical models describing the kaon nucleon interaction in systems with more than two nucleons [31][34]. Information on the nature of the $\Lambda(1405)$ state can be obtained from the upper level transitions of light kaonic atoms, like Li, Be and B [35], (see Sec. 4.1).

- *Transitions to be measured.* We plan to use $^{3,4}He, ^{6,7}Li, ^9Be, ^{10,11}B$ targets to perform measurements of both low level and high level transitions with $\Delta n = 1, 2, ...5$, and energies in the range 10-100 keV.

- *Detector performances and setup.* We plan to perform the above mentioned measurements using two SIDDHARTA-like setups in parallel, to be placed above and below the DAΦNE IP. The first one, devoted to the lowest energy region, will make use of $1\,mm$ thick Silicon Drift Detectors (SDD) having large efficiencies in the 10-40 keV range; the second one will concentrate on the 40-100 keV lines by means of CdTe or CdZnTe devices. $1\,mm$ thick SDD detectors are being built, while R&D CdTe is ongoing in the framework of the Work-Package JRA8-ASTRA of the EU STRONG-2020 project, in which our community is involved [36]. Both detectors have the required energy resolutions (FWHM $\simeq 150 - 200\,eV\,(SDD)\,/\,0,5 - 1\,keV(Cd(Zn)Te)$) to clearly separate all the lines of interest. A simple schematic of the possible setup is shown in Fig. 12 right, where the two replica of the target cell, (partially) surrounded by the holders for the detectors, are shown above and below the IP; two pairs of scintillators, to be used as Kaon Trigger and Luminosity Monitor like in the SIDDHARTA-2 experiment, are as well shown.

- *Luminosity request and feasibility.* The feasibility of both these experiments is grounded on two solid starting points. First, the production of $1\,mm$ thick SDDs has been already financed by the INFN CSN3; in addition, our collaboration already possesses a strong knowledge about their readout electronics, handling and calibration procedure, gathered during the SIDDHARTA and SIDDHARTA-2 experiments. Second, prototypes of Cd(Zn)Te detectors and their related readout electronics will be delivered by the JRA8-ASTRA. Assuming SIDDHARTA-like conditions we estimate a required integrated luminosity of $800\,pb^1$ for kaonic helium and of $400\,pb^{-1}$ for the other targets. This results in an overall 26 months time schedule: 12 months for the design and production of detectors, electronics and mechanical supports, 6 months for the setup calibration, test, mounting and optimization, and 8 months of data taking.

4.2.3. Ultra-high precision measurements of selected exotic atoms (KA3)

- *Expected impact and physics motivation.* A new exciting possibility in the investigation of kaonic atoms is represented by extreme (sub-eV) precision measurements of their transitions. For example, a particularly significant measurement would be the relative difference in the $3d \rightarrow 2p$ transition shifts between K^3He and K^4He (known as the isotopic shift puzzle for the striking difference between the theoretical models predictions) and of their widths, whose measurement with a precision below 1 eV might represent a breakthrough in the field. For a proper determination of these shifts, it is as well necessary to have an accurate determination of the electromagnetic values of the 2p energy levels which, in turn, are influenced by the precision of the K^- mass value, which could be also extracted with sub-eV precision measurements of kaonic atoms. Moreover, it turns out that the systematic uncertainty of the D0-meson mass is also limited by the precision on the charged kaon mass [37][38]. Also, the masses of all excited charmed mesons, whose direct measurements are rather uncertain, e.g. those of $D_1(2420)^0$, $D_4^*(2460)^0$ and $D_{s1}(2536)^{\pm}$, are determined from the fit based on high-precision measurements of mass and mass difference of the D^0, $D^{\pm}$ and $D_s^{\pm}$ states [39]. The precision on the

D^0 mass also impacts on the mixing parameters in the $D^0 - \overline{D^0}$ system [37]. In the long run, a more accurate kaon mass determination may become appealing for first-principle calculations on the lattice [40]. Finally, measurements of very narrow kaonic atoms (few eV or below eV FWHM) transitions from upper levels, from which important information on the $\Lambda(1405)$ nature can be extracted [35], could only be performed with such a high resolution experiment.

- *Transitions to be measured.* To address the scientific questions mentioned above and in Sec. 4.1, we plan to perform simultaneous measurements of $K^{3,4}He(7, 6, 5, 4, 3 \rightarrow 2)$ as well as $KN(12, 11, 10, 9, 8, 7, 6 \rightarrow 7, 6, 5)$ transitions, where the first ones will deliver the isotopic shift and the second ones inputs to the kaon mass precise determination [27], while from both a rich dataset for kaon cascade processes can be retrieved [32]. Measurements of light-Z kaonic atoms with very narrow upper level transitions [35], are also foreseen. All the lines of interest fall in the 6-15 keV range.

- *Detector performances and setup.* To achieve the required challenging precisions, detectors with $FWHM \simeq 10\,eV\,@\,6-10\,keV$ resolution, more than one order of magnitude better than the standard large area solid state devices, we plan to exploit the resolution and efficiency performances of the Highly Annealed Pyrolitic Graphite (HAPG) mosaic crystals based Von Hamos spectrometer, developed by the VOXES collaboration at LNF [41–44]. A drawing of the proposed setup, consisting of 8 spectrometer arms devoted to a specific energy range each, is shown in Fig. 13. Kaons emitted from the IP are first detected by a scintillator and SiPMs based trigger system, before entering in a cylindrical gaseous target cell surrounding the beam pipe, where they form the kaonic atoms; the X-ray photons emitted during the transitions are then measured by a specific energy range spectrometer having a resolution of few eV.
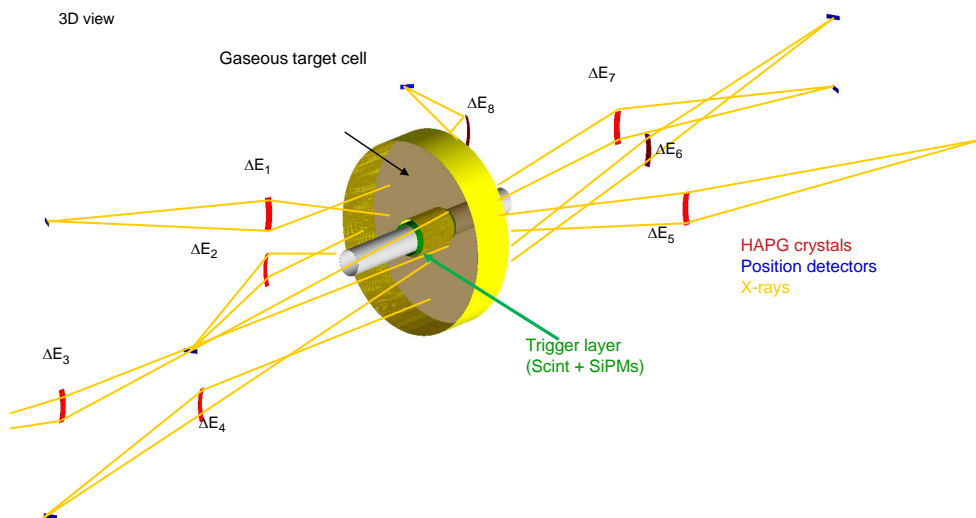

Figure 13: Setup of the KA3 experiment (see text for details).

- *Luminosity request and feasibility.* The foreseen performances of the KA3 experiment are supported by very encouraging preliminary data obtained within the VOXES project [41–44]. Consistent ray-tracing simulations have been performed, allowing a *successful design* and planning of the setup. The in-beam behaviour of the crystals and the position detectors are planned to be assessed in a run in parallel with SIDDHARTA-2. To fulfill the scientific program of KA3, $\simeq 2000\,pb^{-1}$ of delivered luminosity are estimated. A possible time duration of the whole experiment can be arranged in 32 months: 16 months devoted to crystals, detectors and mechanics design and production, 6 months to test and calibrations, 2 months for mounting and, finally, the last 8 months to the data taking.

4.3. Kaon-nuclei interaction studies at the low-energy frontier

4.3.1. Expected impact and physics motivation

The physics of the strong interaction manifests in the dynamics driven by the chiral symmetry breaking of low energy QCD. Explicit symmetry breaking by the mass of the strange quark plays an important role when extending the framework to flavour SU(3). Low-energy interactions of anti-kaons with nucleons and nuclei, measured with the highest possible precision, are excellent probes to explore and improve the understanding of this fundamental topic - the interplay between spontaneous and explicit chiral symmetries breaking. High-precision K-p threshold data, derived from accurate results for kaonic hydrogen from DEAR [3] and recently from SIDDHARTA [4], set important constraints for theoretical approaches. Missing now are precise total and differential cross sections of low-energy kaon-nucleon reactions, because, the available experimental data below 100 MeV/c, are very few and with large errors bars, see for example Fig. 14.

Moreover, kaon induced $\Lambda(1405)$ production on light nuclear targets can provide crucial information to solve the longstanding debate on the nature of the $\Lambda(1405)$ state. In particular the process $K^- d \to \Sigma^0 \pi^0 n$, for a K^- momentum of the order of 120 MeV/c, was investigated in the context of both phenomenological potential approaches [45] and chiral unitary models [46] and was found to be the golden channel to unveil the possible existence of a high mass (1420 MeV/c^2) pole of the $\Lambda(1405)$, and hence to definitely solve this fundamental problem.
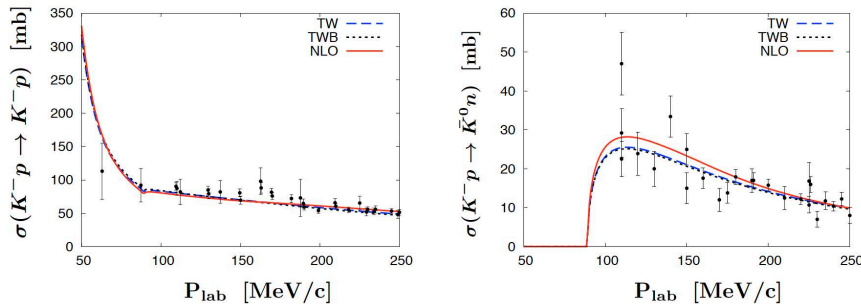

Figure 14: Two examples from [47, 48]: (left) experimental data set for the elastic kaon-proton reaction, (right), the $K^- p \to \overline{K^0} n$ non-elastic channel, both fitted with theoretical models. Data below 100 MeV/c have large error bars or are missing.

4.3.2. Kaon-nucleon elastic scattering KN1

The goal of the KN1 experiment is the measurement of the low-energy scattering process of kaons, and of the $\Lambda(1405)$ kaon induced production, on various targets, such as hydrogen, deuterium, helium-3 and helium-4. The measurements of particles with such low momenta represent a big experimental challenge. The component of the experimental apparatus will be an active Time Projection Chamber (TPC) with a Gas Electron Multiplier (GEM) readout device, which allows the study of kaons interactions directly in the TPC gas/target volume, without additional material. We have already started to develop, in the framework of the EU programmes HadronPhysics3 and STRONG-2020, active target concepts using GEM-TPCs, which are well suited for this type of studies. The experimental setup is made of three detector parts: the kaon monitor, the active target detector (a GEM-based TPC) and the charged kaon detector.

- *The kaon monitor*: consists of plastic scintillator pads (see Fig. 15 left), which are read out on both sides with Silicon Photo-Multipliers (SiPMs). The scintillator pads are arranged around the interaction region, covering the TPC kaon entrance window. The kaon monitor detects the charged kaon-pairs produced via the ϕ-decay, which are emitted back-to-back. This topology allows to setup a clear trigger scheme, with excellent timing (starting point) and in addition allows to reduce background events.

- *The active GEM-TPC* as a low mass target and detector, motivated by the need to study the low energy interactions of kaons with nuclei in a complete way, using an almost massless system. This detection technique requires the use of low-radiation length materials and very pure light gases such
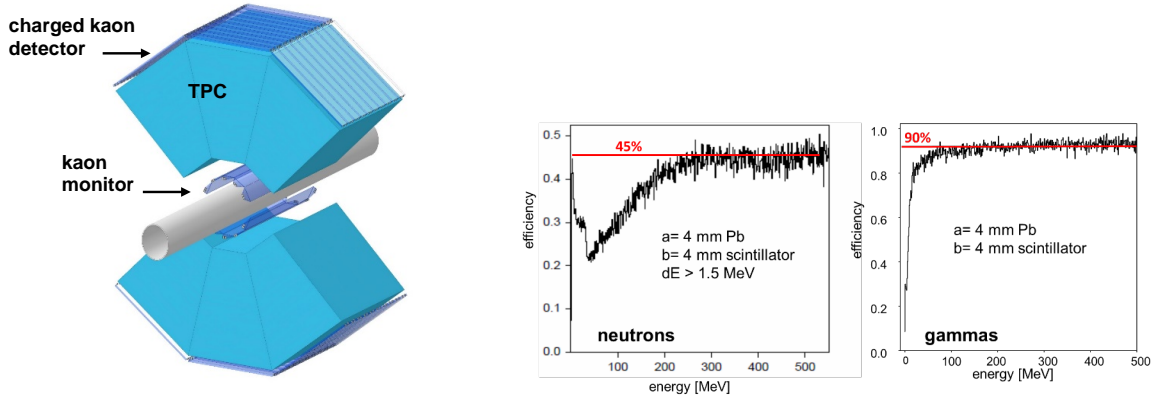
Figure 15: Sketch of the possible setup for the KN-elastic, KN1, experiment (left) and Efficiency simulation within Geant4 of the detector for neutrons and gammas (right).

as hydrogen, deuterium, helium-3, helium-4, etc. To evaluate the GEM-TPC performances, a 10×10 cm^2 prototype with a drift gap of 15 cm has been realized. The detector was tested at the πM1 beam facility of the Paul Scherrer Institut (PSI) with low momentum pions and protons [49]. In addition, tests with pure hydrogen and helium gases without impurities were tested with a triple GEM device at SMI in Vienna in the framework of a diploma thesis [50].

- *The charged kaon detector*: made of plastic scintillator pads, read out with SiPMs, covering the outer part of the TPC window completely. The scintillator pads have to be thick enough to stop all kaons, with the goal to distinguish between negative and positive charged kaons (see Fig. 15).

.

The layout of the KN1 detector system is in an advanced state. The kaon monitor will be quite similar to that already used for SIDDHARTA-2, while the charged kaon detector will use the same components as the Veto-2 detector system of SIDDHARTA-2. The design studies for the GEM-TPC used as active target is almost ready and a first prototype should be built within this year in collaboration with our Japanese colleagues from Tohoku University in Sendai.

4.3.3. Kaon-nuclei interactions (KN2)

To study non-elastic channels, in particular the process: $K^-d \to \Lambda(1405)n \to \Sigma^0\pi^0 n$, it is necessary to the detect neutrons, as well as gammas. The resonant formation of the high mass $\Lambda(1405)$ pole, is predicted in [46] to be enhanced by selecting forward neutrons, with respect to the incident K^-, in the center of mass frame. Therefore, a new detector concept to detect neutral particles is under study. The idea is to use lead plates separated by a liquid scintillator. The scintillation light will be picked-up by wavelengths shifting fibres, which are lead through on both sides of the detector volume and read-out on both sides by SiPMs. Monte Carlo studies (Geant4) have shown (see Fig. 15 right) that such a design is very well suitable for our purpose. In detail, one detector module should have a height of 20 cm and a thickness of 25 cm with a length of 80 cm and consists of 32 layers of lead (4 mm thick) with 4 mm gap between lead layers filled with liquid scintillator. The expected efficiency for neutrons is 45%, while the detection efficiency for gammas 90 %. The detector setup will use the same components as for the KN1 experiment and in addition 20 modules of the lead-scintillator sandwich detector will be placed around the KN1 setup.

We are also studying the feasibility of selected hypernuclei measurements required by theoreticians, by adding HPGe detectors (see KA1) to the setup; this suggestion came out from the discussion during the Strangeness workshop: https://agenda.infn.it/event/25725/overview.

4.3.4. Time schedule

For the KN1 experiment preliminary Monte Carlo simulations have been performed with Geant4 showing that with an integrated luminosity of 10 pb^{-1} per day we will expect $\sim$ 2000 K^-p elastic scattering events within about 30 days. For the proposed programme to measure hydrogen, deuterium, helium-3 and helium-4 a total of four months of beam time is necessary.

For the KN2 experiment Monte Carlo simulations are ongoing. Typical measuring time for one target is in the order of 5-6 weeks with an integrated luminosity of 10 pb^{-1} per day.

4.4. References

[1] M. Zobov, et al., Test of crab-waist collisions at DAΦNE ϕ factory, Phys. Rev. Lett. 104 (2010) 174801. `doi:10.1103/PhysRevLett.104.174801`.

[2] C. Milardi, et al., Results from the DAΦNE high luminosity test, Nuovo Cim. 32 (2009) 379–382. `doi:10.1393/ncc/i2009-10476-6`.

[3] G. Beer, et al., Measurement of the kaonic hydrogen X-ray spectrum, Phys. Rev. Lett. 94 (2005) 212302. `doi:10.1103/PhysRevLett.94.212302`.

[4] M. Bazzi, et al., A New Measurement of Kaonic Hydrogen X-rays, Phys. Lett. B 704 (2011) 113–117. `arXiv:1105.3090`, `doi:10.1016/j.physletb.2011.09.011`.

[5] M. Bazzi, et al., First measurement of kaonic helium-3 X-rays, Phys. Lett. B 697 (2011) 199–202. `arXiv:1010.4631`, `doi:10.1016/j.physletb.2011.02.001`.

[6] M. Bazzi, et al., Kaonic helium-4 X-ray measurement in SIDDHARTA, Phys. Lett. B 681 (2009) 310–314. `doi:10.1016/j.physletb.2009.10.052`.

[7] C. Curceanu, et al., Unlocking the secrets of the kaon-nucleon/nuclei interactions at low-energies: The SIDDHARTA(-2) and the AMADEUS experiments at the DAΦNE collider, Nucl. Phys. A 914 (2013) 251–259. `doi:10.1016/j.nuclphysa.2012.12.128`.

[8] C. Curceanu, et al., Kaonic Atoms to Investigate Global Symmetry Breaking, Symmetry 12 (4) (2020) 547. `doi:10.3390/sym12040547`.

[9] O. Vázquez Doce, et al., K^- absorption on two nucleons and ppK$^-$ bound state search in the Σ^0p final state, Phys. Lett. B 758 (2016) 134–139. `arXiv:1511.04496`, `doi:10.1016/j.physletb.2016.05.001`.

[10] K. Piscicchia, S. Wycech, C. Curceanu, On the K^4He to $Lambda\pi\,^3He$ resonant and non-resonant processes, Nucl. Phys. A 954 (2016) 75–93. `doi:10.1016/j.nuclphysa.2016.05.007`.

[11] K. Piscicchia, et al., First measurement of the K^-n to $\Lambda\pi^-$ non-resonant transition amplitude below threshold, Phys. Lett. B 782 (2018) 339–345. `doi:10.1016/j.physletb.2018.05.025`.

[12] R. Del Grande, et al., K^- multi-nucleon absorption cross sections and branching ratios in Λp and Σ^0p final states, Eur. Phys. J. C 79 (3) (2019) 190. `arXiv:1809.07212`, `doi:10.1140/epjc/s10052-019-6694-7`.

[13] R. Del Grande, et al., Total branching ratio of the K$^-$ two-nucleon absorption in ^{12}C, Phys. Scripta 95 (8) (2020) 084012. `doi:10.1088/1402-4896/ab9ed3`.

[14] A. Gal, E. V. Hungerford, D. J. Millener, Strangeness in nuclear physics, Rev. Mod. Phys. 88 (3) (2016) 035004. `arXiv:1605.00557`, `doi:10.1103/RevModPhys.88.035004`.

[15] A. Gal, Overview of Antikaon-Nuclear Theory and Phenomenology, Prog. Theor. Phys. Suppl. 168 (2007) 556–564. `arXiv:nucl-th/0703098`, `doi:10.1143/PTPS.168.556`.

[16] W. Horiuchi, T. Hyodo, W. Weise, Kaonic deuterium from realistic antikaon-nucleon interaction, EPJ Web Conf. 199 (2019) 03003. `doi:10.1051/epjconf/201919903003`.

[17] L. Tolos, M. Centelles, A. Ramos, The Equation of State for the Nucleonic and Hyperonic Core of Neutron Stars, Publ. Astron. Soc. Austral. 34 (2017) e065. `arXiv:1708.08681`, `doi:10.1017/pasa.2017.60`.

[18] D. Lonardoni, F. Pederiva, S. Gandolfi, Accurate determination of the interaction between Λ hyperons and nucleons from auxiliary field diffusion Monte Carlo calculations, Phys. Rev. C 89 (1) (2014) 014314. `arXiv:1312.3844`, `doi:10.1103/PhysRevC.89.014314`.

[19] A. Drago, A. Lavagno, G. Pagliara, D. Pigato, Early appearance of Δ isobars in neutron stars, Phys. Rev. C 90 (6) (2014) 065809. `arXiv:1407.2843`, `doi:10.1103/PhysRevC.90.065809`.

[20] A. Ramos, J. Schaffner-Bielich, J. Wambach, Kaon condensation in neutron stars, Lect.Notes Phys 578 (2001) 175.

[21] H. Djapo, B.-J. Schaefer, J. Wambac, On the appearance of hyperons in neutron stars, Phys. Rev. C 81 (2010) 035803.

[22] D. Logoteta, I. Vidana, I. Bombaci, Impact of chiral hyperonic three-body forces on neutron stars, Eur. Phys. J. A55 (11) (2019) 207.

[23] D. Lonardoni, A. Lovato, S. Gandolfi, F. Pederiva, Hyperon Puzzle: Hints from Quantum Monte Carlo Calculations, Phys. Rev. Lett 114 (9) (092301) 175.

[24] P. Ribes, A. Ramos, L. Tolos, C. Gonzalez-Boquera, M. Centelles, Interplay between Particles and Hyperons in Neutron Star, Astrophys. J. 883 (2019) 168.

[25] L. Bonanno, A. Sedrakian, Composition and stability of hybrid stars with hyperons and quark color-superconductivity, Astron. Astrophys. 539 (2012) A16.

[26] M. Merafina, F. G. Saturni, C. Curceanu, R. Del Grande, K. Piscicchia, Self-gravitating strange dark matter halos around galaxies, Phys. Rev. D 102 (8) (2020) 083015. `arXiv:2007.03024`, `doi:10.1103/PhysRevD.102.083015`.

[27] M. Tanabashi, et al., Review of Particle Physics, Phys. Rev. D 98 (2018) 030001. `doi:10.1103/PhysRevD.98.030001`.
URL `https://link.aps.org/doi/10.1103/PhysRevD.98.030001`

[28] D. Bosnar, et al., Revisiting the Charged Kaon Mass, Acta Phys. Polon. B 51 (2020) 115–120. `doi:10.5506/APhysPolB.51.115`.

[29] M. Bonesini, The proton radius puzzle, EPJ Web of Conferences 164 (12 2016). `doi:10.1051/epjconf/201716407048`.

[30] C. E. Carlson, The proton radius puzzle, Progress in Particle and Nuclear Physics 82 (2015) 59–77. `doi:10.1016/j.ppnp.2015.01.002`.
URL `http://dx.doi.org/10.1016/j.ppnp.2015.01.002`

[31] C. Curceanu, Strong interaction with strangeness@lnf: a unique opportunity (2021).
URL `https://agenda.infn.it/event/25299/contributions/127688/attachments/78168/100901/StrangenessPrecision_FFF-13jan2021-final.pptx`

[32] T. Koike, Cascade calculation of exotic atoms with many electrons electron population during the cascade of kaonic nitrogen atoms, Genshikaku Kenkyu 49 (2005) 159–164.
URL `http://inis.iaea.org/search/search.aspx?orig_q=RN:36064054`

[33] M. Skurzok, et al., Characterization of the SIDDHARTA-2 luminosity monitor, JINST 15 (10) (2020) P10010. `arXiv:2008.05472`, `doi:10.1088/1748-0221/15/10/P10010`.

[34] E. Friedman, B. Gal, Features of $k^- nn$ interaction in light kaonic atoms (2020).

[35] S. Wycech, B. Loiseau, An Advantage of "Upper Levels", Acta Phys. Polon. B 51 (2020) 109. `doi:10.5506/APhysPolB.51.109`.

[36] Jra8-astra: Advanced ultra-fast solid state detectors for high precision radiation spectroscopy.
URL `http://www.strong-2020.eu/joint-research-activity/jra8-astra.html`

[37] J. P. e. a. Lees, Measurement of the mass of the D^0 meson, Phys. Rev. D 88 (2013) 071104. `doi:10.1103/PhysRevD.88.071104`.
URL `https://link.aps.org/doi/10.1103/PhysRevD.88.071104`

[38] A. Tomaradze, S. Dobbs, T. Xiao, K. K. Seth, G. Bonvicini, High precision measurement of the masses of the D^0 and K_S mesons, Phys. Rev. D 89 (2014) 031501. `doi:10.1103/PhysRevD.89.031501`.
URL `https://link.aps.org/doi/10.1103/PhysRevD.89.031501`

[39] P. D. Group, P. A. e. a. Zyla, Review of Particle Physics, Progress of Theoretical and Experimental Physics 2020 (8), 083C01 (08 2020). `arXiv:https://academic.oup.com/ptep/article-pdf/2020/8/083C01/34673722/ptaa104.pdf`, `doi:10.1093/ptep/ptaa104`.
URL `https://doi.org/10.1093/ptep/ptaa104`

[40] Prelovsek, Sasa, Hadron spectroscopy and interactions from lattice qcd, EPJ Web Conf. 129 (2016) 00018. `doi:10.1051/epjconf/201612900018`.
URL `https://doi.org/10.1051/epjconf/201612900018`

[41] A. Scordo, L. Breschi, C. Curceanu, M. Miliucci, F. Sirghi, J. Zmeskal, High resolution multielement xrf spectroscopy of extended and diffused sources with a graphite mosaic crystal based von hamos spectrometer, J. Anal. At. Spectrom. 35 (2020) 155–168. `doi:10.1039/C9JA00269C`.
URL `http://dx.doi.org/10.1039/C9JA00269C`

[42] A. Scordo, C. Curceanu, M. Miliucci, F. Sirghi, J. Zmeskal, Pyrolitic graphite mosaic crystal thickness and mosaicity optimization for an extended source von hamos x-ray spectrometer, Condensed Matter 4 (2) (2019) 59. `doi:10.3390/condmat4020038`.

[43] A. Scordo, C. Curceanu, M. Miliucci, H. Shi, F. Sirghi, J. Zmeskal, VOXES: a high precision X-ray spectrometer for diffused sources with HAPG crystals in the 2–20 keV range, JINST 13 (04) (2018) C04002. `doi:10.1088/1748-0221/13/04/C04002`.

[44] A. Scordo, H. Shi, C. Curceanu, M. Miliucci, F. Sirghi, J. Zmeskal, VOXES, a new high resolution X-ray spectrometer for low yield measurements with diffused sources, Acta Phys. Polon. B48 (2017) 1715. `doi:10.5506/APhysPolB.48.1715`.

[45] J. Esmaili, Y. Akaishi, T. Yamazaki, Resonant formation of Lambda(1405) by stopped-K- absorption in deuteron, Phys. Rev. C 83 (2011) 055207. `arXiv:0909.2573`, `doi:10.1103/PhysRevC.83.055207`.

[46] D. Jido, E. Oset, T. Sekihara, Kaon induced $\Lambda(1405)$ production on a deuteron target at DAFNE, Eur. Phys. J. A 47 (2011) 42. `arXiv:1008.4423`, `doi:10.1140/epja/i2011-11042-3`.

[47] Y. Ikeda, T. Hyodo, W. Weise, Chiral SU(3) theory of antikaon-nucleon interactions with improved threshold constraints, Nucl. Phys. A 881 (2012) 98–114. `arXiv:1201.6549`, `doi:10.1016/j.nuclphysa.2012.01.029`.

[48] Y. Ikeda, T. Hyodo, W. Weise, Chiral su(3) theory of antikaon–nucleon interactions with improved threshold constraints, Nuclear Physics A 881 (2012) 98–114, progress in Strangeness Nuclear Physics. `doi:https://doi.org/10.1016/j.nuclphysa.2012.01.029`.
URL `https://www.sciencedirect.com/science/article/pii/S0375947412000607`

[49] M. Poli Lener, G. Corradi, C. Curceanu, D. Tagnani, A. Romero Vidal, J. Zmeskal, Performances of an Active Target GEM-Based TPC for the AMADEUS Experiment, Mod. Instrum. 4 (2015) 32–41. `doi:10.4236/mi.2015.43004`.

[50] A. Franke, Studies of a triple GEM detector setup, Master thesis, University of Vienna (2015).